nature genetics

ARTICLES

https://doi.org/10.1038/s41588-021-00827-w

Shared heritability of human face and brain shape

Sahin Naqvi[1,2,20] ✉, Yoeri Sleyp[3,20], Hanne Hoskens[3,4], Karlijne Indencleef[4,5], Jeffrey P. Spence[2], Rose Bruffaerts[6,7,8], Ahmed Radwan[4,9], Ryan J. Eller[10], Stephen Richmond[11], Mark D. Shriver[12], John R. Shaffer[13,14], Seth M. Weinberg[13,14,15], Susan Walsh[10], James Thompson[16], Jonathan K. Pritchard[2], Stefan Sunaert[4,9], Hilde Peeters[3], Joanna Wysocka[1,17,18,21] ✉ and Peter Claes[3,4,5,19,21] ✉

Evidence from model organisms and clinical genetics suggests coordination between the developing brain and face, but the role of this link in common genetic variation remains unknown. We performed a multivariate genome-wide association study of cortical surface morphology in 19,644 individuals of European ancestry, identifying 472 genomic loci influencing brain shape, of which 76 are also linked to face shape. Shared loci include transcription factors involved in craniofacial development, as well as members of signaling pathways implicated in brain–face cross-talk. Brain shape heritability is equivalently enriched near regulatory regions active in either forebrain organoids or facial progenitors. However, we do not detect significant overlap between shared brain–face genome-wide association study signals and variants affecting behavioral–cognitive traits. These results suggest that early in embryogenesis, the face and brain mutually shape each other through both structural effects and paracrine signaling, but this interplay may not impact later brain development associated with cognitive function.

The human cerebral cortex forms the outer layer of gray matter of the brain and underpins cognitive function. It is characterized by complex folding patterns varying between species and individuals[1,2]. Family- and twin-based studies indicate substantial heritability of brain shape[3,4], and a recent genome-wide association study (GWAS) found that brain shape is highly polygenic with genetic correlations to a broad range of neuropsychiatric disorders and behavioral–cognitive phenotypes[5]. These studies focused on predefined, univariate measures of brain shape, such as total or regional surface area, extracted from structural magnetic resonance imaging (MRI) scans[6], which cannot capture morphological complexities of the cortical surface. We recently developed a data-driven approach to phenotyping complex, multidimensional traits[7]; this multivariate approach, when applied to facial surface images, revealed numerous loci with no previously known role in human face shape variation[7,8]. Here, we implemented this approach to discover associations between common genetic variants and brain shape, using MRI data from middle-aged participants in the UK Biobank (UKB) who were free of disease diagnosis.

In addition to sharing complex morphologies, the development of the brain and face is highly integrated due to shared developmental lineage, spatial proximity and signaling cross-talk between both structures[9]. Early in embryonic development, the rostral end of the ectodermally derived neural tube gives rise to the forebrain, which in turn gives rise to the cerebrum that encompasses the cerebral cortex[10]. Just before forebrain formation, a subset of neuroepithelial cells within the neural folds give rise to facial progenitor cells called cranial neural crest cells (CNCCs)[11]. Following specification, CNCCs undergo an epithelial-to-mesenchymal transition and migrate ventrally[12], giving rise to most of the craniofacial skeleton and connective tissue[13]. Early brain growth rates can modulate both positioning and outgrowth of the facial prominences[14,15], as well as induce flexion and bone deposition of CNCC-derived basicranial bones[16,17] and neurocranial sutures[18,19], respectively. Finally, paracrine factors secreted by either the developing forebrain[20–23] or CNCCs[24–26] modulate the facial or brain development, respectively.

These physical and molecular interactions have been detailed by studies in developing chick and mouse embryos, but are also supported by widespread co-occurrence of neurodevelopmental and craniofacial malformations in rare human syndromes[27]. This phenomenon was noticed by DeMyer et al.[28] in 1964, who coined the phrase 'the face predicts the brain' to describe correlations between the severity of brain and face malformations in patients with holoprosencephaly. While in some cases this co-occurrence may be caused by pleiotropic gene functions, a number of human syndromes have been mapped to genes functioning in brain–face cross-talk through paracrine signaling[29–31]. Nonetheless, close developmental links between face and brain are underappreciated;

[1]Department of Chemical and Systems Biology, Stanford University School of Medicine, Stanford, CA, USA. [2]Departments of Genetics and Biology, Stanford University School of Medicine, Stanford, CA, USA. [3]Department of Human Genetics, KU Leuven, Leuven, Belgium. [4]Medical Imaging Research Center, University Hospitals Leuven, Leuven, Belgium. [5]Department of Electrical Engineering, ESAT/PSI, KU Leuven, Leuven, Belgium. [6]Department of Neurosciences, KU Leuven, Leuven, Belgium, Hasselt University, Hasselt, Belgium. [7]Neurology Department, University Hospitals Leuven, Leuven, Belgium, Hasselt University, Hasselt, Belgium. [8]Biomedical Research Institute Hasselt University Hasselt Belgium, Hasselt University, Hasselt, Belgium. [9]Department of Imaging and Pathology, Translational MRI, KU Leuven, Leuven, Belgium. [10]Department of Biology, Indiana University Purdue University Indianapolis, Indianapolis, IN, USA. [11]Applied Clinical Research and Public Health, School of Dentistry, Cardiff University, Cardiff, UK. [12]Department of Anthropology, Pennsylvania State University, State College, PA, USA. [13]Department of Human Genetics, University of Pittsburgh, Pittsburgh, PA, USA. [14]Department of Oral and Craniofacial Sciences, Center for Craniofacial and Dental Genetics, University of Pittsburgh, Pittsburgh, PA, USA. [15]Department of Anthropology, University of Pittsburgh, Pittsburgh, PA, USA. [16]Department of Psychology, George Mason University, Fairfax, VA, USA. [17]Department of Developmental Biology, Stanford University School of Medicine, Stanford, CA, USA. [18]Howard Hughes Medical Institute, Stanford University School of Medicine, Stanford, CA, USA. [19]Murdoch Children's Research Institute, Melbourne, Victoria, Australia. [20]These authors contributed equally: Sahin Naqvi, Yoeri Sleyp. [21]These authors jointly supervised this work: Joanna Wysocka, Peter Claes. ✉e-mail: naqvi@stanford.edu; wysocka@stanford.edu; peter.claes@kuleuven.be

whether and how they extend to common human genetic variation influencing brain and face shape is unknown.

Results

Multivariate genome-wide association study of brain shape. We adapted our previously published data-driven phenotyping approach[7] to brain shape, as measured by MRI scans of 19,644 individuals in the UKB. Participants included were of primarily European ancestry, such that results do not pertain to cross-population differences in brain shape. We focused on the mid-cortical surface (midway between the white–gray matter interface and the pial surface with the cerebrospinal fluid, as extracted using FreeSurfer[6]), which we refer to as brain shape. Using mid-cortical surfaces represented by a mesh of three-dimensional (3D) vertices, the method segments brain shape in a global-to-local manner, yielding brain segments at different hierarchical levels of scale. Within each segment, principal-component analysis (PCA) is used to describe effects in multivariate shape space explaining between-individual variation, and canonical correlation analysis (CCA) is used to define, for each variant, the linear combination of principal components (PCs) maximally associated with SNP dosage. Unsurprisingly, a GWAS of left and right hemispheres from the same individuals showed highly concordant results (Supplementary Fig. 1); therefore, we performed subsequent analyses using left–right hemisphere averaged data.

Applying this pipeline to UKB MRI data defined 285 hierarchical segments (Fig. 1 and Supplementary Table 1), decomposing brain shape into different levels of detail, from larger brain segments with integrated variation, to smaller brain segments with local effects. Each hierarchical level is a bipartition of its parent; the first level consisted of the entire brain, while the second and third levels segmented the whole brain into halves and quadrants, respectively, and the final, ninth level resulted in numerous smaller segments (Fig. 1b). Many smaller segments from the seventh hierarchical level onwards were discarded due to small surface areas, resulting in fewer total segments than the 511 (2^9-1) expected. Nevertheless, the ninth hierarchical level yielded a substantial number (74) of retained segments; a tenth level would contribute few additional segments (Supplementary Fig. 2). The segmentation broadly agreed with the commonly used Desikan-Killiany[32], Destrieux[33] and Glasser[34] brain atlases (Supplementary Fig. 3). Before GWAS, we adjusted for covariates including total brain volume, height, body mass index (BMI), sex and population structure, as well as performing standard SNP filtering and quality control (Methods). Applying linkage disequilibrium score regression (LDSC)-based heritability estimation to each segment's GWAS (see Methods and Supplementary Note for details on extension to multivariate traits) yielded intercept values close to 1 (range across segments 0.987–1.007, mean 1.001; Supplementary Table 1), indicating minimal confounding by population structure or cryptic relatedness. In total, we conducted 285 multivariate GWASs using CCA, each corresponding to one segment. Around 38,630 SNPs showed genome-wide significant ($P<5\times10^{-8}$) associations with brain shape in at least one segment; of these, 23,413 reached study-wide significance ($P<2.07\times10^{-10}$ correcting for the number of effective GWASs, estimated by permutation; Methods) in at least one segment. Collapsing these SNPs into independent signals based on linkage disequilibrium (LD) and distance yielded 472 and 242 loci reaching genome-wide and study-wide significance, respectively (Supplementary Table 2). Most of the 472 loci showed effects on multiple segments (305/472, 65%), and many showed effects on multiple quadrants (158/472, 33%; Fig. 1 and Supplementary Table 2), consistent with global-to-local effects at multiple levels of brain shape. Masking of associations from progressively higher hierarchical levels revealed that segments from higher levels contributed a substantial fraction of associations; for example, segments beyond the first three levels contributed 169 and 55 loci reaching genome-wide and study-wide significance, respectively (Extended Data Fig. 1). Associations between the 472 loci and brain shape were depleted from the frontal lobe segments (except for the most anterior orbitofrontal cortex) and enriched in the occipital and temporal lobe segments (Supplementary Fig. 4), mostly in agreement with point-wise heritability estimates (Extended Data Fig. 2).

We assessed the overlap between the 472 loci and previous GWAS results of brain surface areas or subcortical volumes[5,35–39]. The 472 loci recapitulated 27–78% of the associations reported in previous studies; the highest overlap of 78% was reported in a recent study of univariate brain surface area[5], the phenotype most comparable to the shape measures studied here (Table 1). Of the 472 loci, 121 overlapped with those reported in previous studies on brain surface area or subcortical volume, while 351 represent previously undescribed associations with brain morphology. To assess the reproducibility of the 472 loci on the same shape measures, we analyzed MRI data from the Adolescent Brain Cognitive Development (ABCD) study[40]. Of the 472 loci, 466 were tested for replication (Methods). At a false discovery rate (FDR) of 5%, we replicated at least one associated segment for 305 of 466 (65.4%) loci, and 2,645 of 3,586 (73.8%) locus–segment combinations (Supplementary Table 3). We observed consistent rates when subdividing based on the hierarchical level of the segments being replicated, albeit with a slight decrease in replication rate at higher levels (Extended Data Fig. 3). These replication rates are notable given the substantial age difference of the ABCD cohort (9–10 years versus 40–70 years in the UKB). The high reproducibility of GWAS results between the two cohorts suggests that, despite the known continued growth and morphological changes of the brain throughout adolescence and into adulthood[41], many of the observed associations with brain shape originate during development and are maintained throughout life.

We next used functional mapping and annotation of GWAS (FUMA)[42] and the genomic regions enrichment of annotations tool (GREAT)[43] to identify pathways enriched among genes near the 472 loci, as well as curated gene panels used to guide disease diagnoses[44] to identify disease associations (Methods). As expected, we found strong enrichment for brain-specific processes (neurogenesis, axonogenesis, neuron differentiation, nervous system development and neuron projection guidance), morphogenesis-related processes (anatomical structure morphogenesis and animal organ morphogenesis) and neurodevelopmental disorders (intellectual disability, malformations of cortical development and ciliopathies). We also observed a weak enrichment of terms related to formation and closure of the neural tube, suggesting that early developmental events impact adult brain shape. Surprisingly, we also observed strong enrichment of terms related specifically to CNCC development and migration, as well as weaker enrichment of broader terms encompassing skeletal system development, chondrogenesis and osteogenesis (Supplementary Data 1). Furthermore, we found strong and weak enrichments for craniosynostosis (premature closer of the cranial bone sutures) and clefting gene panels, respectively. These enrichments suggest a link between variation in brain shape and craniofacial skeletal development.

Loci affecting both brain and face shape. To more directly test for sharing of genetic effects between brain and face shape, we intersected the 472 loci described in this study with 203 loci previously associated with face shape in individuals of European ancestry through a similar, open-ended phenotyping approach[8]. Thirty-seven of the loci for brain shape were linked ($r^2>0.2$) to at least one of the face shape loci, significantly above random expectation ($P=2.03\times10^{-22}$, odds ratio = 10.6) and greater than the overlap with other traits that have similar numbers of genome-wide significant associations in the NHGRI-EBI GWAS Catalog[45] (Extended Data Fig. 4). Identifying signals showing a genome-wide

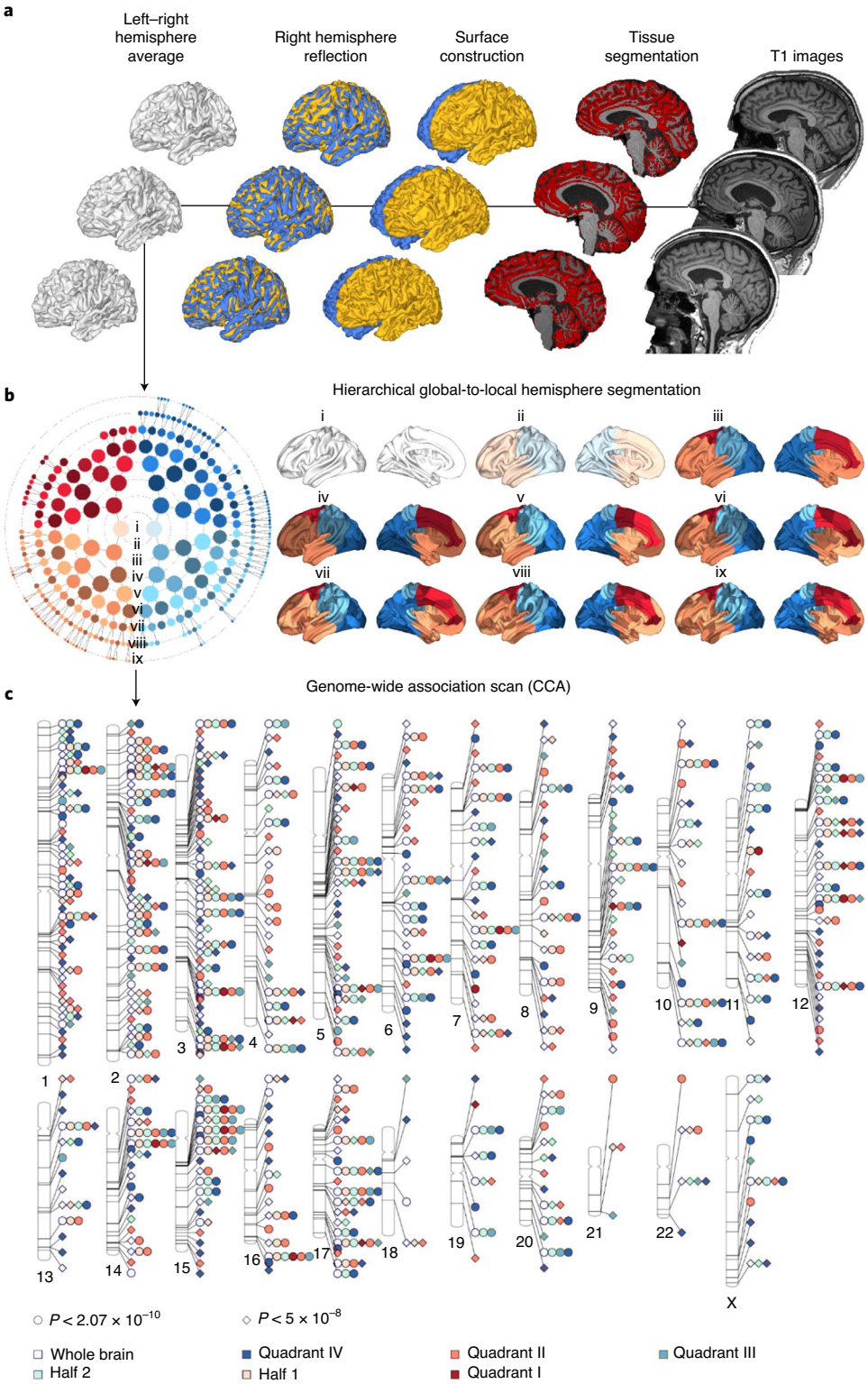

Fig. 1 | Multivariate genome-wide association study of brain shape. a, Upstream processing of UKB MRI images. **b**, In the polar dendrogram (left), each concentric ring of filled circles corresponds to a hierarchical level (i–ix) shown on the right, and the filled circle colors correspond to the respective segments in the same hierarchical level. **c**, Ideogram showing genomic locations and regional effects of 472 genome-wide significant loci for brain shape. Circles and diamonds represent associations passing the study-wide or genome-wide significance thresholds. Colors represent broad regions of the brain with the indicated effects.

significant association with one of brain or face shape and a suggestive ($P < 5 \times 10^{-7}$) association with the other resulted in 76 brain–face shared loci (Fig. 2a).

Genes near the 76 brain–face shared loci were strongly enriched for disease associations, including 'skeletal disorders' and 'hearing and ear disorders', consistent with the contribution of CNCCs to

Table 1 | Overlap between previous GWAS results of brain surface areas or subcortical volumes with GWAS results of brain shape in this study

Study	Number of loci tested	Number of lead SNPs with $P < 5 \times 10^{-8}$	Number of proxy SNPs with $P < 5 \times 10^{-8}$	Overlap (%)
Subcortical combined[31–34]	65	15	18	27.6
Grasby et al.[5]	301	195	236	78.4
Zhao et al.[35]	494	212	273	55

'Subcortical combined' refers to a combined set of loci from four studies of subcortical volume measures[35–38].

craniofacial skeleton and ear structures. We next manually scanned the 76 brain–face shared loci for genes with known roles in craniofacial or brain development from human syndromes and/or knockout mouse models (Supplementary Table 4). We observed that many of the shared brain–face loci included genes encoding transcription factors (TFs) involved in neural crest formation and/or craniofacial skeletal development. Some of those TFs (for example, DLX5/6, SOX9, ZEB2, ZIC2, ZIC3 and TCF4) have known functions in both neural crest and brain development, and this pleiotropy may account for the shared brain–face genetic signals. However, other shared brain–face signals are associated with TFs thought to function primarily during neural crest rather than brain development, and whose mutation causes specific craniofacial defects; those TFs include ALX1 and ALX4 (associated with frontonasal dysplasias[46,47]), TWIST1 (associated with Saethre–Chotzen syndrome[48,49]), PAX3 (associated with Waardenburg syndrome[50]) and TFAP2B (associated with CHAR syndrome[51]). Consistent with the primary role of these TFs in facial development, transcriptome analysis showed high expression in in vitro-derived human CNCCs and their chondrocyte derivatives[52], but low or no expression in either glia or neurons of human forebrain organoids spanning a range of developmental stages[53] (Fig. 2b). These observations suggest that genetic variants affecting key craniofacial TFs have a greater than previously appreciated impact on brain shape.

Interactions between face and brain can be architectural, with the forebrain acting as a structural support for facial development, and facial skeletal structures flexing to accommodate early brain growth[54]. However, these interactions can also involve paracrine signaling, with fibroblast growth factor (FGF), Hedgehog and bone morphogenetic protein (BMP) pathways known to mediate the signaling from the developing brain to the face[20–22]. Interestingly, genes encoding members of all three pathways, FGF (*FGF2*, *FGF13*, *FGF18* and *SPRY2*), Hedgehog (*PTCH1*) and BMP (*BMP2* and *BMP4*) are among the shared brain–face loci. For example, mutations in *PTCH1*, encoding the receptor for the sonic hedgehog ligand, cause holoprosencephaly[55], a congenital, structural forebrain anomaly with associated craniofacial malformations. Conversely, CNCCs secrete anti-BMP signaling molecules that modulate forebrain development[24,25]; expression of these BMP antagonists is dependent on the SIX family of TFs, whose perturbation in CNCCs leads to both craniofacial malformations and secondary pre-otic brain defects[56]. *SIX1* and *SIX4* are also among the 76 brain–face shared loci (Fig. 2a). Furthermore, genes linked to other signaling pathways, including Wnt (*DAAM1*, *DAAM2*, *TNKS*, *AHI1*, *FBXW11* and *MCC*) and transforming growth factor beta (*LEMD3* and *PPP2R3A*), are among the shared brain–face loci. Not unexpectedly, and in contrast to craniofacial TFs, signaling pathway ligands, receptors and regulators are variably expressed between in vitro-derived CNCCs and brain organoids (Fig. 2b).

Phenotypically, these highlighted loci largely affect brain shape in the frontal and temporal lobes, and face shape in the forehead and nose, as exemplified by *PAX3* and *ALX1* (Fig. 2c), consistent with the physical proximity of the frontonasal prominence and the forebrain during development. Phenotypic effects distinct from this pattern include effects of variants near *BMP4* and *DLX6* on jaw and chin morphology, consistent with their known roles in mandibular development[57,58], and effects of variants near *PTCH1* on occipital lobe morphology (Fig. 2c). Together, these results suggest that both cell-intrinsic mechanisms and paracrine signaling pathways contribute to the substantial number of loci with shared associations with brain and face shape.

Genome-wide sharing of signals with neuropsychiatric disorders and behavioral–cognitive traits. We next asked whether the brain–face overlap among genome-wide significant loci held across the genome, also considering GWASs of neuropsychiatric disorders and behavioral–cognitive traits. LDSC can estimate genetic correlations between univariate traits using signed summary statistics[59]. However, this approach is not applicable to unsigned statistics yielded by CCA. We therefore applied an alternative method of assessing genome-wide sharing of signals between two GWASs, summarizing SNP *P* values within approximately independent LD blocks and computing Spearman correlations between the two summarized profiles (Methods). When applied to pairs of univariate GWAS results, the Spearman correlation method was largely concordant with, albeit generally smaller in magnitude than, unsigned estimates of LDSC-estimated genetic correlations (Extended Data Fig. 5), indicating that it is a conservative, robust measure for quantifying genome-wide sharing of GWAS signals.

We first assessed sharing of association signals between 63 face segments and 285 brain segments (Supplementary Table 5). All four main facial quadrants, representing shape variation within the forehead, nose, lower face (mandible and cheeks) and philtrum, respectively, showed the most sharing with frontal lobe segments, particularly the most anterior portions such as the rostral prefrontal cortex, and the least sharing with parietal lobe segments (Fig. 3a). Furthermore, among the facial quadrants, the forehead and nose showed more sharing with frontal lobe segments than the philtrum and lower face. These genome-wide correlations are consistent with the phenotypic effects of top brain–face shared loci (Fig. 2c and Supplementary Fig. 5).

We next assessed sharing of signals with other brain-related traits. We used publicly available genome-wide summary statistics for a range of neuropsychiatric disorders, behavioral–cognitive traits and subcortical brain volumes from studies other than UKB, since our Spearman correlation measure does not control for sample overlap (Supplementary Table 6). As approximate negative controls, we used four immune-related diseases shown to have minimal genetic correlation with schizophrenia and bipolar disorder[60]. Subcortical volumes showed the most sharing with brain shape in the corresponding regions, but the magnitude of these correlations was relatively low (on par with sharing between brain and face shape), indicating that our multivariate GWAS approach detects effects beyond those resulting from changes in relative subcortical volume (Fig. 3b). We found that disorders with primarily developmental etiology showed substantial sharing with brain shape in regions previously linked to these disorders. For instance, schizophrenia and attention deficit hyperactivity disorder (ADHD) showed sharing with shape variation in the primary auditory[61,62] and prefrontal cortex[63] regions, respectively. In contrast, we did not observe this association for Alzheimer's disease, caused by plaque buildup and neurodegeneration much later in life. Behavioral–cognitive traits such as intelligence, neuroticism and worry showed broader patterns of sharing with brain shape, reflecting the involvement of distributed cortical regions in these traits[64–66] (Fig. 3b).

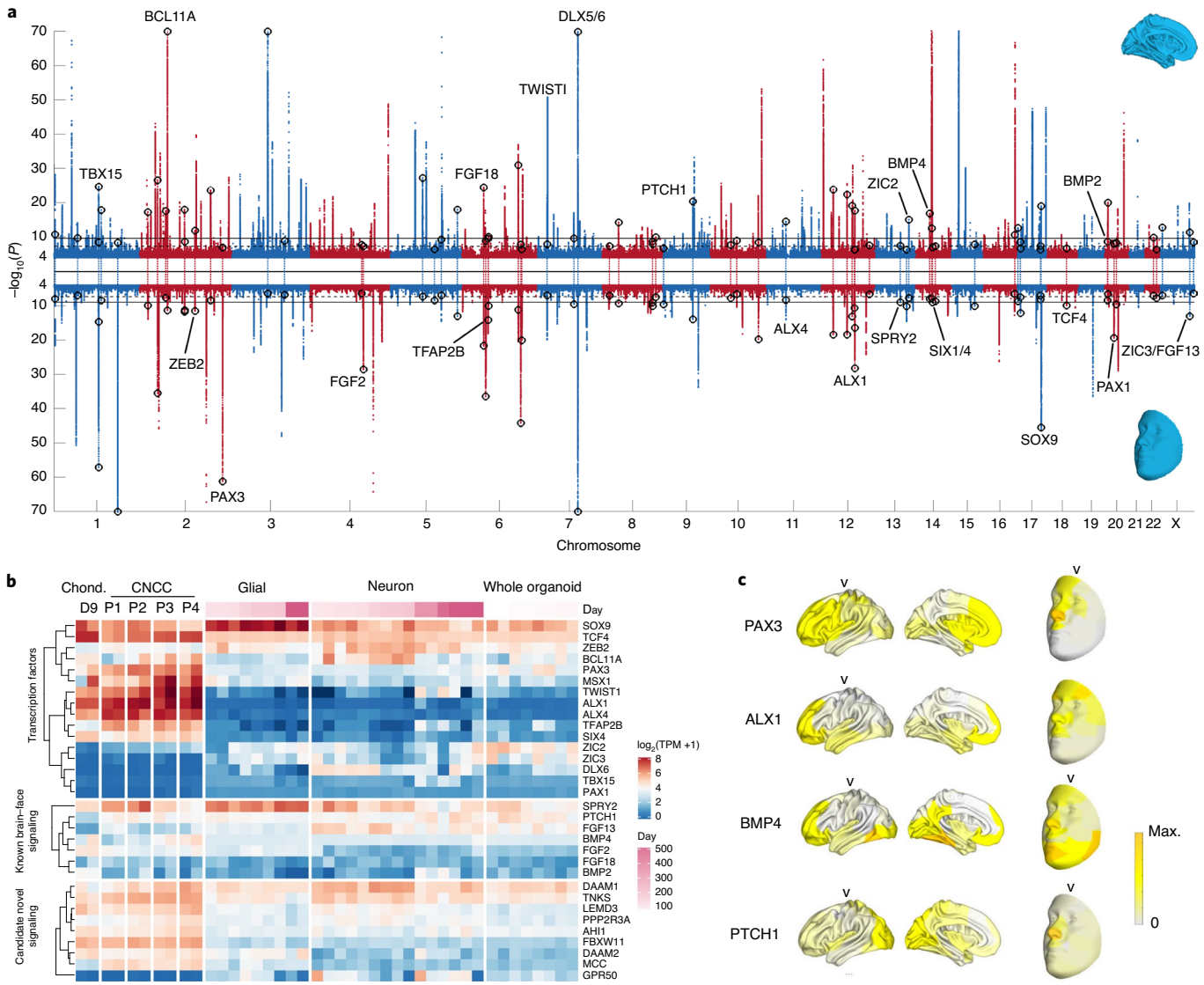

Fig. 2 | Loci affecting both brain and face shape. a, Miami plot of GWAS results for brain (top) and face (bottom) shape. For each SNP, *P* values aggregated across all brain or face segments were plotted. All 76 loci reaching genome-wide significance ($P < 5 \times 10^{-8}$) in one study and genome-wide suggestive significance ($P < 5 \times 10^{-7}$) in the other are highlighted by unfilled circles. Right-tailed, one-sided *P* values were computed based on CCA chi-squared statistics; exact *P* values are available in Supplementary Table 4. Loci near candidate genes highlighted in the text and in **b** and **c** are labeled, generally on the side where they show greater significance of association. **b**, Expression (in transcripts per million, TPM) of candidate genes near brain–face shared loci in CNCCs of different passages, representing different stages of maturation, from early (postnatal day (P) 1) to late (P4) and their chondrocyte (Chond. D9) derivatives[52] (left), and 3D forebrain organoids at various stages of differentiation[53] (right), further sorted into glial or neuronal lineages or profiled as whole organoids. **c**, Regional phenotypic effects of four candidate loci, showing effects of linked SNPs on brain (left) or face (right) shape. Segments shown are of hierarchical level v; $-\log_{10}(P$ values) are normalized to the maximum at each locus. Full face and brain images from all 76 brain–face shared loci corresponding to all hierarchical levels can be found online (Data Availability).

Sharing between brain shape and the immune diseases was generally lower than with neuropsychiatric disorders, behavioral–cognitive traits or subcortical volumes, but reached significance for type 1 diabetes (T1D) and rheumatoid arthritis (RA; Fig. 3c). This overlap may be because these immune traits have genetic correlation with brain-related traits other than those tested previously (schizophrenia and bipolar disorder), as suggested by a significant genetic correlation between RA and intelligence (Extended Data Fig. 6).

Finally, we compared the degree to which face shape shares signals with neuropsychiatric disorders, behavioral–cognitive traits and subcortical volumes. Brain shape shares significant (5% FDR) signal with most neuropsychiatric traits, as well as all behavioral–cognitive and subcortical volume traits analyzed. In contrast, face shape does not show significant sharing with any of the neuropsychiatric disorders or behavioral–cognitive traits, and significant but weaker sharing with the subcortical volume measures (Fig. 3c). To confirm these patterns using univariate approaches, we performed a GWAS on the most heritable individual PCs of full brain or face shape and computed genetic correlations using LDSC. Although genetic correlation estimates were noisy due to low heritability of univariate shape GWAS, they agreed with our Spearman correlation measure, finding nonzero genetic correlations between both brain and face shape and subcortical volumes, and between brain shape and both autism spectrum disorder and bipolar disorder (Extended Data Fig. 7). Thus, the substantial sharing of signals between brain and face shape (Fig. 3a) appears to be mostly independent of

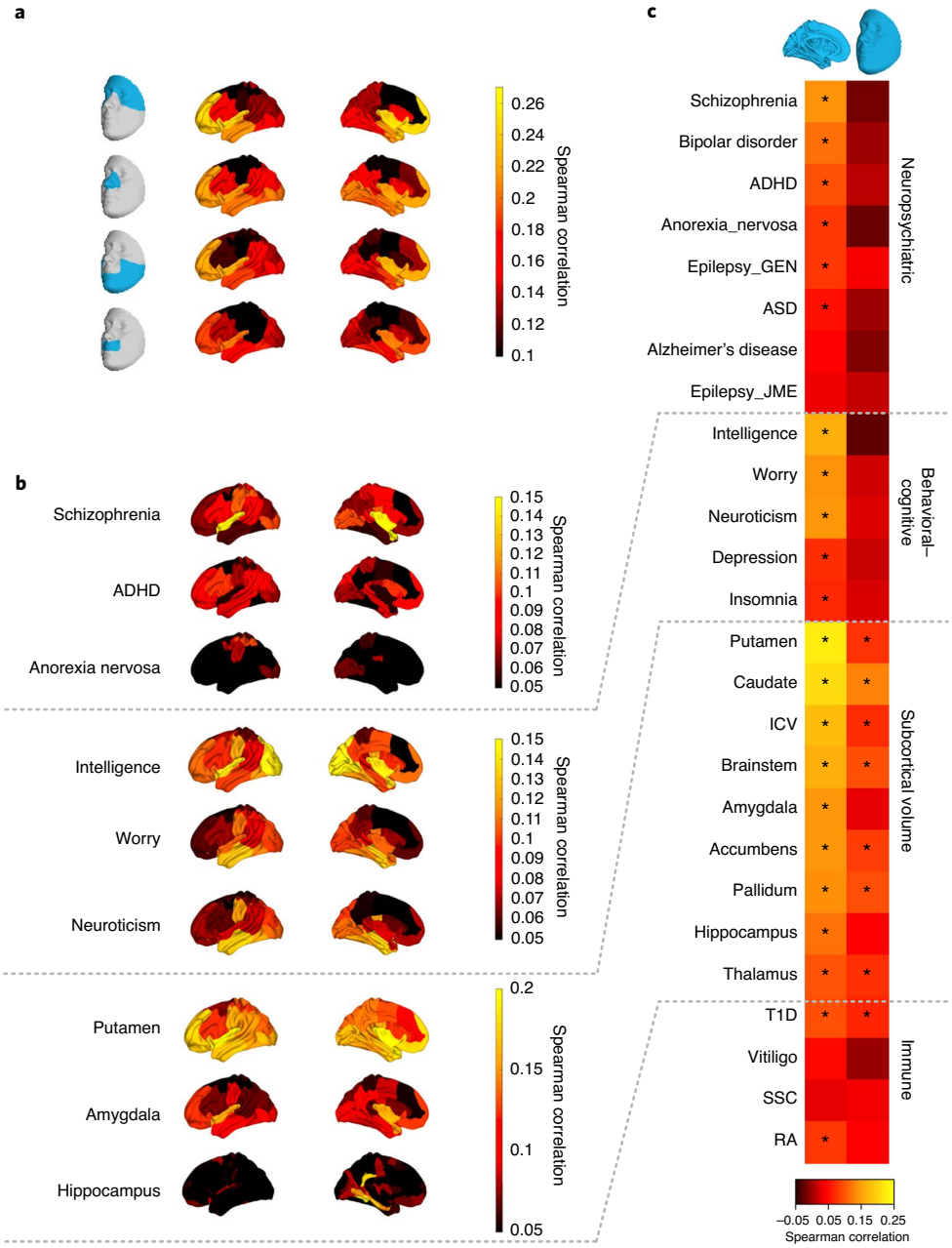

Fig. 3 | Genome-wide sharing of signals with neuropsychiatric disorders and behavioral–cognitive traits. Genome-wide sharing of signals between any two given GWASs was assessed by Spearman correlation of LD block-average SNP $-\log_{10}(P$ values) (Methods). **a**, Spearman correlations between GWAS data of indicated facial quadrants and brain segments. **b**, Spearman correlations between GWAS data of selected neuropsychiatric disorders, behavioral–cognitive traits, subcortical volume measures and brain segments or select immune traits. All brain segments in **a** and **b** were from hierarchical-level v segmentation, with the exception of the hippocampus, where hierarchical-level vi segmentation showed a strong correlation of shape of the hippocampal region with volume. **c**, Spearman correlations between shape effects on the full brain (left) or face (right) with the indicated traits. *5% FDR based on bootstrapped *P* value (Methods). Images of brain–trait correlations at all six hierarchical levels can be found online ('Data Availability'). GEN, generalized epilepsy; JME, juvenile myoclonic epilepsy; ICV, intracranial volume; SSC, systemic sclerosis.

neuropsychiatric disorder risk and behavioral–cognitive traits, perhaps because mutual influences of face and brain shape on each other involve phenotypic effects on brain shape distinct from those influencing neuropsychiatric disorder risk and behavioral–cognitive traits.

Cell types influencing brain and face shape. Our results thus far suggest that a substantial fraction of brain shape variation is underpinned by face shape, but that these observed effects are largely independent of effects shared between brain shape and other cognitive traits. To test this idea further, we sought to identify the cell types most enriched for heritability of brain shape, face shape and other cognitive traits. Partitioning heritability into cell-type-specific functional annotations via stratified LD score regression (S-LDSC) can prioritize trait-relevant cell types, but was developed for univariate traits[67]; we thus sought to extend the theoretical framework of S-LDSC to multivariate traits such as our brain and face shape GWAS. We demonstrated that when applying unstratified

LDSC[59] to χ^2 statistics obtained from multivariate traits with independent dimensions and further corrected for dimensionality, the LDSC-estimated heritability equals the average heritability of the component univariate traits (Methods and Supplementary Note), a finding that we validated through heritability estimation of each PC making up the full face (Extended Data Fig. 8). By extension, heritability enrichments obtained by applying S-LDSC on multivariate, corrected χ^2 statistics partitioned by annotation represent the average heritability enrichment for each component univariate trait (Methods and Supplementary Note).

We collected genome-wide data on open chromatin (inferred from the assay for transposase-accessible chromatin using sequencing (ATAC–seq)) and active regulatory regions (inferred from chromatin immunoprecipitation followed by sequencing (ChIP–seq) of histone marks) from a variety of cell types and tissues, including in vitro-derived CNCCs and their chondrocyte derivatives[52,68], embryonic craniofacial tissue at different stages of development[69], neuronal and glial cells from 3D forebrain organoids at various differentiation stages[53] and both fetal and adult brain tissue[70]. We quantified brain and face shape heritability enrichments for these cell-type-specific annotations (Supplementary Data 2). Face shape showed significant (5% FDR) heritability enrichment specific to regulatory regions in craniofacial cell types (mean *z*-score 4.58; Fig. 4a). Brain shape showed significant and comparable heritability enrichments for regulatory regions in craniofacial cell types and tissues, brain organoids and fetal brain tissue (mean *z*-scores 4.23, 3.23 and 3.33, respectively; Fig. 4b). Within brain organoids, the strongest enrichments were for early-stage glial cells and whole organoids (mean *z*-score 4.11; Extended Data Fig. 9), consistent with an important role for radial glial cells in corticogenesis and in agreement with enrichments of brain surface area heritability[5]. The strong enrichments for craniofacial cell types, which were more significant than organoid enrichments in the orbitofrontal and medial temporal lobes (Supplementary Fig. 6), suggest that heritability shared between brain and face shape is mediated primarily by CNCCs and their derivatives early in embryonic development. Consistent with this idea, quantifying brain shape heritability enrichments after removing the 76 brain–face shared loci resulted in decreased enrichment for CNCCs (*z*-score difference −0.68) and slightly increased enrichment for early-stage glial cells (*z*-score difference 0.23; Extended Data Fig. 10).

Finally, we quantified heritability enrichments for neuropsychiatric disorders, behavioral–cognitive traits and subcortical volumes. Neuropsychiatric disorders and behavioral–cognitive traits showed enrichment patterns distinct from those of brain shape, with significant enrichment for both fetal and adult brain tissue (mean *z*-scores 2.17 and 2.64, respectively), and broad enrichment across stages and cell types of brain organoids (mean *z*-score 2.46). In contrast to brain shape, these traits showed no enrichment for craniofacial cell types or tissues (mean *z*-score −0.92; Fig. 4c). Subcortical volumes showed mixed enrichment patterns, with some regions (amygdala and caudate) similar to those of multivariate brain shape and others (putamen) closer to those of neuropsychiatric disorders and behavioral–cognitive traits. These results suggest that while much of the shared genetic variation between brain and face shape is mediated by regulatory regions in CNCCs and their craniofacial derivatives, variation in these regions does not appear to impact neuropsychiatric disorder risk or other behavioral–cognitive traits.

Discussion

Here, we applied multivariate phenotyping to discover numerous loci underlying common variation in brain shape. While these loci broadly implicate known pathways in brain development, the precise mechanisms by which they modulate brain shape are unknown, suggesting further avenues of investigation. As part of our study, we extended techniques for estimating genome-wide and partitioned heritability, originally developed for univariate traits, to multivariate traits. We anticipate that these and similar extensions will become increasingly useful with the greater availability of high-dimensional imaging or morphological data in large sample sizes.

We found a striking convergence of common genetic variation affecting brain and face shape, at least in part mediated by regulatory regions active in CNCCs and their derivatives. These observations suggest a larger than previously appreciated role of the face in shaping development of the brain and its morphological variation between individuals. However, these shared genetic effects do not appear to substantially impact neuropsychiatric disorder risk or cognitive functions. Our results are therefore consistent with a model whereby CNCCs and their derived cranial structures substantially influence brain shape through both physical interactions and paracrine signaling early in embryogenesis, but later shaping of cortical morphology, through processes such as the folding of the cortical surface[71], has a greater impact on cognitive traits. Nevertheless, we cannot exclude the possibility that future GWASs of cognitive traits show more substantial overlap with brain–face shared genetic effects, perhaps due to alternative trait definitions or to greater statistical power.

A number of developmental mechanisms could mediate shared brain–face genetics. One potential contribution comes from the common neuroepithelial origins of the two structures, with genes influencing growth, patterning and cell fate decisions within the neural plate ultimately affecting cell allocation within distinct parts of the brain and face; examples of such neural plate genes within brain–face shared loci include *ZIC2* and *ZIC3* (refs. [72–74]). Another potential mechanism entails common genetic variation modulating expression of genes with independent roles in both brain and face development. *SOX9*, encoding a TF with key functions in neural crest development and chondrogenesis, but which is also required for gliogenesis[75], is an attractive candidate for this mechanism. Nonetheless, the primary impact of brain–face shared genetic effects on facial regions from the frontonasal prominence and anterior forebrain regions of the brain suggests additional, proximity-based mechanisms, which can be either structural, or mediated by paracrine signaling. While brain and face development must be tightly coordinated, the former is thought to have greater structural effects on craniofacial development, as the forebrain can serve as structural support for facial development[54] as well as induce flexion of the basicranium and bone deposition at coronal sutures through growth-dependent tensile forces[17,18,54]. However, we find multiple brain–face shared loci near TFs with known, cell-intrinsic roles in, and expression specific to, CNCCs and their derivatives. Furthermore, mutations in genes encoding these TFs result in malformations of the frontal facial skeleton,

Fig. 4 | Partitioned heritability enrichments based on cell-type-specific regulatory annotations. Heritability enrichment *z*-scores, as estimated by S-LDSC, of multivariate shape for the first seven face segments (**a**), multivariate shape for the first seven brain segments (**b**), excluding segment 4 which had low heritability, neuropsychiatric disorders (**c**), behavioral–cognitive traits (**d**) and subcortical volume measures (**e**). Heritability enrichments were estimated for annotations based on open chromatin (based on ATAC–seq), regulatory regions (based on ChIP–seq) of multiple histone modifications), or a combination of the two. Annotations for the indicated samples, representing in vitro-derived cell types, primary tissues, or a combination of both (see Methods for source papers), were added to the S-LDSC baseline model, and the resulting *z*-score was scaled by column to visualize relative enrichments between traits. *5% FDR based on unscaled *z*-scores. hESC, human embryonic stem cell; iPSC, induced pluripotent stem cell.

such as coronal synostosis (*TWIST1*)[48,49] or frontonasal dysplasias (*ALX1* and *ALX4*)[46,47]. One explanation for these results is that these TFs control regulatory programs ultimately modulating the ability of the craniofacial skeleton to respond to and accommodate brain growth, causing subtle changes in brain shape. It is also possible, however, that these TFs exert some phenotypic effects on

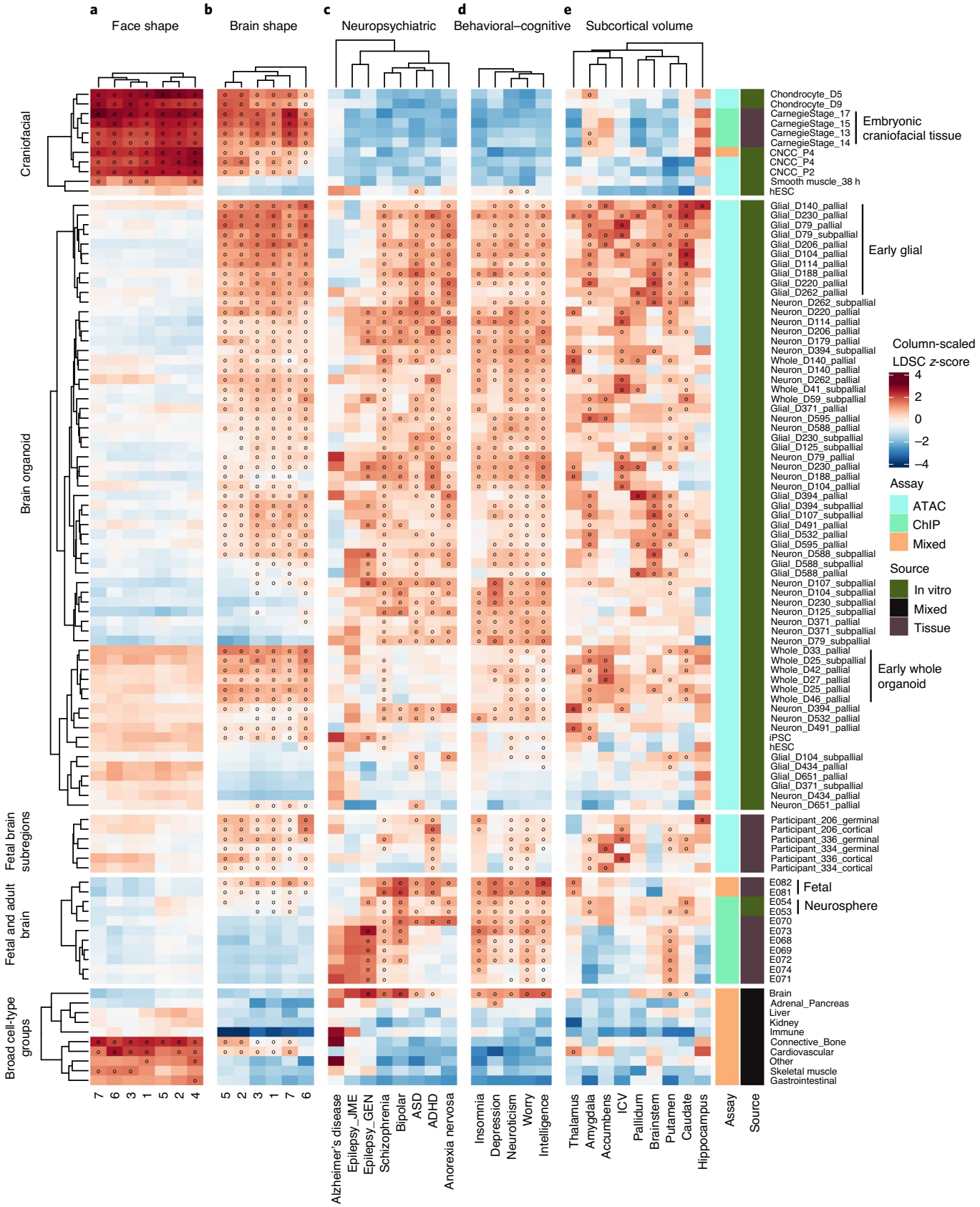

brain shape by regulating expression of signaling ligands secreted from the face. For example, CNCCs secrete BMP antagonists that modulate forebrain development by blocking BMP and FGF production in the anterior neural ridge[24,25]. BMP antagonist production in CNCCs is regulated by the SIX family TFs[56], with *SIX1/SIX4* lying near a shared brain–face GWAS signal (Fig. 2a). In the reverse direction, studies in chick embryos have shown that Fgf, Shh and BMP ligands are secreted by the forebrain and regulate the formation of the frontonasal ectodermal zone, a signaling center that in turn patterns the frontonasal prominence of the developing face[20–22,76]. Notably, our study implicates all three of these signaling pathways, nominating specific ligands and receptors whose modulation may be associated with the brain–face cross-talk. Furthermore, our study nominates other pathways, such as Wnt and transforming growth factor beta, for roles in paracrine brain–face signaling. Altogether, we uncovered common genetic variants yielding numerous candidate molecular players whose diverse mechanistic roles in mediating brain–face interactions during development can be examined in future studies.

Relationships of facial shape with cognitive and personality traits have fascinated humans since ancient times, from the ancient Greeks, who introduced 'physiognomy' to describe a practice of assessing one's personality from facial appearance[77], through the Vedic traditions of Samudrika Shastra[78] and to the Chinese art of face reading[79]. The concept of physiognomy was revived in the 18th century by Johan Kaspar Lavater, and later led to a related pseudoscientific theory, phrenology, popularized by Franz Josef Gall. Both theories have a troubled history, as they have been used to justify racial discrimination and eugenic theories[80,81]. While the original formation of physiognomy has been debunked, modern studies have found correlations between facial width-to-height ratios and aggressive tendencies[82], with regrettable renewed efforts in using machine learning approaches to detect such correlations raising serious ethical concerns[83,84]. Our results argue that while the ancient human intuition of a close relationship between the face and brain has genetic support at the morphological level, there does not appear to be genetic evidence for the supposed predictive value of face shape in behavioral–cognitive traits, which formed the core of physiognomy and related theories.

Online content

Any methods, additional references, Nature Research reporting summaries, source data, extended data, supplementary information, acknowledgements, peer review information; details of author contributions and competing interests; and statements of data and code availability are available at https://doi.org/10.1038/s41588-021-00827-w.

Received: 29 August 2020; Accepted: 16 February 2021;
Published online: 05 April 2021

References

1. Lui, J. H., Hansen, D. V. & Kriegstein, A. R. Development and evolution of the human neocortex. *Cell* **146**, 18–36 (2011).
2. Gu, J. & Kanai, R. What contributes to individual differences in brain structure? *Front. Hum. Neurosci.* **8**, 1–6 (2014).
3. Strike, L. et al. Genetic complexity of cortical structure: differences in genetic and environmental factors influencing cortical surface area and thickness. *Cereb. Cortex* **29**, 952–962 (2019).
4. Wen, W. et al. Distinct genetic influences on cortical and subcortical brain structures. *Sci. Rep.* **6**, 1–11 (2016).
5. Grasby, K. L. et al. The genetic architecture of the human cerebral cortex. *Science* **367**, eaay6690 (2020).
6. Fischl, B. FreeSurfer. *Neuroimage* **62**, 774–781 (2012).
7. Claes, P. et al. Genome-wide mapping of global-to-local genetic effects on human facial shape. *Nat. Genet.* **50**, 414–423 (2018).
8. White, J. D. et al. Insights into the genetic architecture of the human face. *Nat. Genet.* **53**, 45–53 (2021).
9. Marcucio, R., Hallgrimsson, B. & Young, N. M. Facial morphogenesis: physical and molecular interactions between the brain and the face. *Curr. Top. Dev. Biol.* **115**, 299–320 (2015)
10. Stiles, J. & Jernigan, T. L. The basics of brain development. *Neuropsychol. Rev.* **20**, 327–348 (2010).
11. Simões-Costa, M. & Bronner, M. E. Establishing neural crest identity: a gene regulatory recipe. *Development* **142**, 242–257 (2015).
12. Theveneau, E. & Mayor, R. Neural crest delamination and migration: from epithelium-to-mesenchyme transition to collective cell migration. *Dev. Biol.* **366**, 34–54 (2012).
13. Santagati, F. & Rijli, F. M. Cranial neural crest and the building of the vertebrate head. *Nat. Rev. Neurosci.* **4**, 806–818 (2003).
14. Diewert, V. M. A morphometric analysis of craniofacial growth and changes in spatial relations during secondary palatal development in human embryos and fetuses. *Am. J. Anat.* **167**, 495–522 (1983).
15. Boughner, J. C. et al. Short-faced mice and developmental interactions between the brain and the face. *J. Anat.* **213**, 646–662 (2008).
16. Lieberman, D. E., Hallgrímsson, B., Liu, W., Parsons, T. E. & Jamniczky, H. A. Spatial packing, cranial base angulation and craniofacial shape variation in the mammalian skull: testing a new model using mice. *J. Anat.* **212**, 720–735 (2008).
17. Hallgrímsson, B., Lieberman, D. E., Liu, W., Ford-Hutchinson, A. F. & Jirik, F. R. Epigenetic interactions and the structure of phenotypic variation in the cranium. *Evol. Dev.* **9**, 76–91 (2007).
18. Herring, S. W. & Teng, S. Strain in the braincase and its sutures during function. *Am. J. Phys. Anthropol.* **112**, 575–593 (2000).
19. Carver, E. A., Oram, K. F. & Gridley, T. Craniosynostosis in Twist heterozygous mice: a model for Saethre–Chotzen syndrome. *Anat. Rec.* **268**, 90–92 (2002).
20. Foppiano, S., Hu, D. & Marcucio, R. S. Signaling by bone morphogenetic proteins directs formation of an ectodermal signaling center that regulates craniofacial development. *Dev. Biol.* **312**, 103–114 (2007).
21. Marcucio, R. S., Cordero, D. R., Hu, D. & Helms, J. A. Molecular interactions coordinating the development of the forebrain and face. *Dev. Biol.* **284**, 48–61 (2005).
22. Chong, H. J. et al. Signaling by SHH rescues facial defects following blockade in the brain. *Dev. Dyn.* **241**, 247–256 (2012).
23. Kaucka, M. et al. Signals from the brain and olfactory epithelium control shaping of the mammalian nasal capsule cartilage. *eLife* **7**, e34465 (2018).
24. Le Douarin, N. M., Brito, J. M. & Creuzet, S. Role of the neural crest in face and brain development. *Brain Res. Rev.* **55**, 237–247 (2007).
25. Le Douarin, N. M., Couly, G. & Creuzet, S. E. The neural crest is a powerful regulator of pre-otic brain development. *Dev. Biol.* **366**, 74–82 (2012).
26. Aguiar, D. P., Sghari, S. & Creuzet, S. The facial neural crest controls fore- and midbrain patterning by regulating Foxg1 expression through Smad1 activity. *Development* **141**, 2494–2505 (2014).
27. Plummer, J. T., Gordon, A. J. & Levitt, P. The genetic intersection of neurodevelopmental disorders and shared medical comorbidities—relations that translate from bench to bedside. *Front. Psychiatry* **7**, 1–8 (2016).
28. DeMyer, W., Zeman, W. & Palmer, C. G. The face predicts the brain: diagnostic significance of median facial anomalies for holoprosencephaly (arhinencephaly). *Pediatrics* **34**, 256–263 (1964).
29. Muenke, M. & Cohen, M. M. J. Genetic approaches to understanding brain development: holoprosencephaly as a model. *Ment. Retard. Dev. Disabil. Res. Rev.* **6**, 15–21 (2000).
30. Muenke, M. & Beachy, P. A. Genetics of ventral forebrain development and holoprosencephaly. *Curr. Opin. Genet. Dev.* **10**, 262–269 (2000).
31. Balk, K. & Biesecker, L. G. The clinical atlas of Greig cephalopolysyndactyly syndrome. *Am. J. Med. Genet. A* **146A**, 548–557 (2008).
32. Desikan, R. S. et al. An automated labeling system for subdividing the human cerebral cortex on MRI scans into gyral-based regions of interest. *Neuroimage* **31**, 968–980 (2006).
33. Destrieux, C., Fischl, B., Dale, A. & Halgren, E. Automatic parcellation of human cortical gyri and sulci using standard anatomical nomenclature. *Neuroimage* **53**, 1–15 (2010).
34. Glasser, M. F. et al. A multimodal parcellation of human cerebral cortex. *Nature* **536**, 171–178 (2016).
35. Hibar, D. P. et al. Common genetic variants influence human subcortical brain structures. *Nature* **520**, 224–229 (2015).
36. Adams, H. H. H. et al. Novel genetic loci underlying human intracranial volume identified through genome-wide association. *Nat. Neurosci.* **19**, 1569–1582 (2016).
37. Hibar, D. P. et al. Novel genetic loci associated with hippocampal volume. *Nat. Commun.* **8**, 13624 (2017).
38. Satizabal, C. L. et al. Genetic architecture of subcortical brain structures in 38,851 individuals. *Nat. Genet.* **51**, 1624–1636 (2019).
39. Zhao, B. et al. Genome-wide association analysis of 19,629 individuals identifies variants influencing regional brain volumes and refines their

genetic co-architecture with cognitive and mental health traits. *Nat. Genet.* **51**, 1637–1644 (2019).
40. Casey, B. J. et al. The adolescent brain cognitive development (ABCD) study: imaging acquisition across 21 sites. *Dev. Cogn. Neurosci.* **32**, 43–54 (2018).
41. Giedd, J. N. et al. Brain development during childhood and adolescence: a longitudinal MRI study. *Nat. Neurosci.* **2**, 861–863 (1999).
42. Watanabe, K., Taskesen, E., van Bochoven, A. & Posthuma, D. Functional mapping and annotation of genetic associations with FUMA. *Nat. Commun.* **8**, 1826 (2017).
43. McLean, C. Y. et al. GREAT improves functional interpretation of *cis*-regulatory regions. *Nat. Biotechnol.* **28**, 495–501 (2010).
44. Martin, A. R. et al. PanelApp crowdsources expert knowledge to establish consensus diagnostic gene panels. *Nat. Genet.* **51**, 1560–1565 (2019).
45. MacArthur, J. et al. The new NHGRI-EBI Catalog of published genome-wide association studies (GWAS Catalog). *Nucleic Acids Res.* **45**, D896–D901 (2017).
46. Uz, E. et al. Disruption of *ALX1* causes extreme microphthalmia and severe facial clefting: expanding the spectrum of autosomal-recessive *ALX*-related frontonasal dysplasia. *Am. J. Hum. Genet.* **86**, 789–796 (2010).
47. Kayserili, H. et al. *ALX4* dysfunction disrupts craniofacial and epidermal development. *Hum. Mol. Genet.* **18**, 4357–4366 (2009).
48. Howard, T. D. et al. Mutations in *TWIST*, a basic helix-loop-helix transcription factor, in Saethre–Chotzen syndrome. *Nat. Genet.* **15**, 36–41 (1997).
49. Ghouzzi, V. E. L. et al. Mutations of the *TWIST* gene in the Saethre–Chotzen syndrome. *Nat. Genet.* **15**, 42–46 (2000).
50. Tassabehji, M. et al. Mutations in the *PAX3* gene causing Waardenburg syndrome type 1 and type 2. *Nat. Genet.* **3**, 26–30 (1993).
51. Zhao, F. et al. Novel *TFAP2B* mutations that cause Char syndrome provide a genotype–phenotype correlation. *Am. J. Hum. Genet.* **69**, 695–703 (2001).
52. Long, H. K. et al. Loss of extreme long-range enhancers in human neural crest drives a craniofacial disorder. *Cell Stem Cell* **27**, 765–783 (2020).
53. Trevino, A. E. et al. Chromatin accessibility dynamics in a model of human forebrain development. *Science* **367**, eaay1645 (2020).
54. Marcucio, R. S., Young, N. M., Hu, D. & Hallgrimsson, B. Mechanisms that underlie co-variation of the brain and face. *Genesis* **49**, 177–189 (2011).
55. Ming, J. E. et al. Mutations in *PATCHED-1*, the receptor for SONIC HEDGEHOG, are associated with holoprosencephaly. *Hum. Genet.* **110**, 297–301 (2002).
56. Garcez, R. C., Le Douarin, N. M. & Creuzet, S. E. Combinatorial activity of *Six1/2/4* genes in cephalic neural crest cells controls craniofacial and brain development. *Cell. Mol. Life Sci.* **71**, 2149–2164 (2014).
57. Liu, W. et al. Threshold-specific requirements for Bmp4 in mandibular development. *Dev. Biol.* **283**, 282–293 (2005).
58. Shimizu, M. et al. Probing the origin of matching functional jaws: roles of *Dlx5/6* in cranial neural crest cells. *Sci. Rep.* **8**, 14975 (2018).
59. Bulik-Sullivan, B. K. et al. LD score regression distinguishes confounding from polygenicity in genome-wide association studies. *Nat. Genet.* **47**, 291–295 (2015).
60. Pouget, J. G. et al. Cross-disorder analysis of schizophrenia and 19 immune-mediated diseases identifies shared genetic risk. *Hum. Mol. Genet.* **28**, 3498–3513 (2019).
61. Kompus, K. et al. The role of the primary auditory cortex in the neural mechanism of auditory verbal hallucinations. *Front. Hum. Neurosci.* **7**, 144 (2013).
62. Mørch-Johnsen, L. et al. Auditory cortex characteristics in schizophrenia: associations with auditory hallucinations. *Schizophr. Bull.* **43**, 75–83 (2016).
63. Hoogman, M. et al. Brain imaging of the cortex in ADHD: a coordinated analysis of large-scale clinical and population-based samples. *Am. J. Psychiatry* **176**, 531–542 (2019).
64. Assem, M., Blank, I. A., Mineroff, Z., Ademoglu, A. & Fedorenko, E. Activity in the frontoparietal multiple-demand network is robustly associated with individual differences in working memory and fluid intelligence. *Cortex* https://doi.org/10.1016/j.cortex.2020.06.013 (2020).
65. Cai, H., Zhu, J. & Yu, Y. Robust prediction of individual personality from brain functional connectome. *Soc. Cogn. Affect. Neurosci.* **15**, 359–369 (2020).
66. Saviola, F. et al. Trait and state anxiety are mapped differently in the human brain. *Sci. Rep.* **10**, 11112 (2020).
67. Finucane, H. K. et al. Partitioning heritability by functional annotation using genome-wide association summary statistics. *Nat. Genet.* **47**, 1228–1235 (2015).
68. Prescott, S. L. et al. Enhancer divergence and *cis*-regulatory evolution in the human and chimp neural crest. *Cell* **163**, 68–83 (2015).
69. Wilderman, A., VanOudenhove, J., Kron, J., Noonan, J. P. & Cotney, J. High-resolution epigenomic atlas of human embryonic craniofacial development. *Cell Rep.* **23**, 1581–1597 (2018).
70. Kundaje, A. et al. Integrative analysis of 111 reference human epigenomes. *Nature* **518**, 317–330 (2015).
71. Gregory, M. D. et al. Regional variations in brain gyrification are associated with general cognitive ability in humans. *Curr. Biol.* **26**, 1301–1305 (2016).
72. Nagai, T. et al. Zic2 regulates the kinetics of neurulation. *Proc. Natl Acad. Sci. USA* **97**, 1618–1623 (2000).
73. Elms, P., Siggers, P., Napper, D., Greenfield, A. & Arkell, R. Zic2 is required for neural crest formation and hindbrain patterning during mouse development. *Dev. Biol.* **264**, 391–406 (2003).
74. Inoue, T., Ota, M., Mikoshiba, K. & Aruga, J. Zic2 and Zic3 synergistically control neurulation and segmentation of paraxial mesoderm in mouse embryo. *Dev. Biol.* **306**, 669–684 (2007).
75. Stolt, C. C. et al. The Sox9 transcription factor determines glial fate choice in the developing spinal cord. *Genes Dev.* **17**, 1677–1689 (2003).
76. Hu, D. & Marcucio, R. S. Neural crest cells pattern the surface cephalic ectoderm during FEZ formation. *Dev. Dyn.* **241**, 732–740 (2012).
77. Boys-Stones, G., Elsner, J., Ghersetti, A., Hoyland, R. & Repath, I. *Seeing the Face, Seeing the Soul: Polemon's Physiognomy from Classical Antiquity to Medieval Islam* (OUP, 2007).
78. Zysk, K. G. *Conjugal Love in India: Ratiâsâastra and Ratiramaòna: Text, Translation and Notes* (Brill, 2002)
79. Mar, T. T. *Face Reading: The Chinese Art of Physiognomy* (Dodd, Mead, 1974)
80. Gray, R. T. *About Face: German Physiognomic Thought From Lavater to Auschwitz* (Wayne State University Press, 2004)
81. Collins, A. F. The enduring appeal of physiognomy: physical appearance as a sign of temperament, character and intelligence. *Hist. Psychol.* **2**, 251–276 (1999).
82. Haselhuhn, M. P., Ormiston, M. E. & Wong, E. M. Men's facial width-to-height ratio predicts aggression: a meta-analysis. *PLoS ONE* **10**, 1–10 (2015).
83. Wu, X. & Zhang, X. Automated inference on criminality using face images. Preprint at https://arxiv.org/abs/1611.04135 (2016).
84. Wu, X. & Zhang, X. Responses to critiques on machine learning of criminality perceptions. Preprint at https://arxiv.org/abs/1611.04135 (2016).

Methods

UK Biobank data preprocessing. The UKB project encompasses ~500,000 British volunteers with informed consent containing genetics, nonimaging variables and brain imaging data acquired using a fixed protocol[85]. Hereby, brain T1-weighted MRI scans of the UKB, as well as genotyping and covariate information (for example, sex, age, height and weight), were used as the discovery dataset. We utilized release v1.5 (August 2018), which holds a cohort of 21,780 participants. This cohort was composed of an adult population (40 to 70 years old, mean of 60 years old), with slightly more females than males (51.6% versus 48.4%, respectively), a predominantly self-reported white British ancestry (97.1%), and an average BMI of 26.6.

For 21,780 participants, we processed raw MRI data for a surface-based analysis of the cortex using the following four-step procedure. Further details for each step are provided in the Supplementary Note.

First, the cortical surfaces were segmented and reconstructed from the MRI volumetric data using the 'recon-all' command (FreeSurfer[86] v.6.0.0; https://surfer.nmr.mgh.harvard.edu/). In this step, 20,409 images were processed successfully.

Second, to obtain a minimally preprocessed pipeline similar to the one of the Human Connectome Project (HCP; http://www.humanconnectomeproject.org/), the Connectivity Informatics Technology Initiative file format (CIFTIFY; https://github.com/edickie/ciftify/ and https://www.nitrc.org/projects/cifti/) was used to convert FreeSurfer's recon-all command output to a HCP-style file format and structure[87].

Third, from the CIFTIFY output, we selected the mid-cortical surface of the left and right hemispheres, which is the surface that runs at the mid-distance between the white surface (at the interface between gray and white matter) and the pial surface (the external cortical surface)[88], using the Conte69 atlas (http://brainvis.wustl.edu/wiki/index.php//Caret:Atlases/Conte69_Atlas). The mid-cortical surface does not overrepresent or underrepresent gyri or sulci[89], but is otherwise an arbitrary choice.

Fourth, as quality control for each hemisphere, we checked the resulting mid-cortical surfaces for mesh artifacts in a semiautomatic manner. All images passed this quality-control procedure, yielding 20,407 processed images.

For the list of 20,407 individuals with preprocessed images, we selected genomic data from the UKB, which consisted of the version 3 (March 2018) imputed SNP genotypes, imputed to the Haplotype Reference Consortium and merged UK10K and 1000 Genomes (phase 3) panels. See the Supplementary Note for more details on filtering of SNPs and individuals based on ancestry and relatedness. This resulted in 9,705,931 filtered SNPs for GWAS analysis on 19,670 unrelated individuals of European descent.

For the list of 19,670 participants with preprocessed brain and genetic data, we collected the following covariates to control for during statistical testing: genetic sex, age, age squared, height, weight, diastolic blood pressure, systolic blood pressure and the first 20 genetic PCs. Furthermore, the following imaging-specific parameters were included, according to work by Elliot et al.[90]: volumetric scaling from T1 head image to standard space, *xyz* position of brain mask in scanner coordinates, *z* position of table/coil in scanner coordinates, date of attending assessment center and name of assessment center (coded as a dummy variable for each of the 21 centers). See the Supplementary Note for more details on covariate-based filtering of individuals. Next, to symmetrize brain shape, the right hemisphere was reflected to the side of the left hemisphere, by changing the sign of the *x*-coordinate for all of the 29,759 3D vertices on the surface of the right hemisphere. We performed a generalized Procrustes superimposition[91], thus eliminating differences in position, orientation and scale (measured by centroid size) of all left and right hemispheres pooled together. We computed the symmetric brain component as the vertex-wise averaged brain surface of paired and superimposed left and right hemispheres. This resulted in a final discovery dataset of 19,644 participants containing preprocessed MRI imaging data on the mid-cortical symmetrized surface, 9,705,931 imputed SNPs and 54 covariates.

Adolescent Brain Cognitive Development Study data preprocessing. The ABCD Study (https://abcdstudy.org/about/) is a longitudinal study following brain development and health through adolescence[40]. A total of 11,411 MRI scans with additional information on sex and age were available from the data release of April 2019 and, of those, 11,393 images were processed successfully using the four-step imaging preprocessing described above.

In total, 10,627 individuals from the ABCD dataset provided genetic data on 517,724 SNP variants. These were imputed via the Odyssey[92] pipeline using the SHAPEIT4 (ref. [93]) and IMPUTE5 (ref. [94]) workflows to phase and impute, respectively. The Haplotype Reference Consortium[95] reference panel was used for imputation. Quality control before phasing and imputation included using the Imputation preparation program by the McCarthy Group (https://www.well.ox.ac.uk/~wrayner/tools/) to check and fix strand, alleles, position and reference/alternative problems, as well as removing ambiguous A/T and G/C SNPS with minor allele frequencies greater than 0.4. See Supplementary Note for more details on phasing, imputation and ancestry-based selection. These steps resulted in a final replication dataset of 4,470 individuals with preprocessed MRI imaging data, representing brain shape, 15.3 million imputed SNPs and 7 covariates (sex, age and the first 5 genetic PCs). The minimum and maximum ages of participants in this final replication dataset were 8.9 years and 11 years, respectively, with a mean age of 9.9 years. Approximately 46.5% were women and 53.5% were men.

Auxiliary trait genome-wide association study summary statistics. We collected publicly available genome-wide summary statistics for 26 auxiliary traits encompassing neuropsychiatric disorders[96–101], behavioral–cognitive traits[102–104], subcortical volume measures[36–38] and immune-related disorders[105–108] with limited genetic correlation with schizophrenia or bipolar disorder[60]. In Supplementary Table 6, we provide links to relevant publications and URLs for these summary statistics.

Point-wise SNP-heritability estimation of the mid-cortical surface. For each of the 29,759 vertices of the averaged mid-cortical 3D surfaces in the UKB, we computed a multivariate (*x*, *y* and *z* coordinate per vertex), narrow-sense heritability from common SNP variants using a linear mixed model (LMM). A genomic relationship matrix modeled as random effects in the LMM was computed from LD-pruned SNPs (PLINK 1.9; window size of 50, step size of 5, 0.2 r^2). The first ten genetic PCs and additional covariates (sex, age, height, weight and diastolic and systolic blood pressure) were modeled as fixed effects in the LMM. We used the open-source software SNPLib (https://github.com/jiarui-li/SNPLIB/)[109], whose implementation is equivalent to that of GCTA[110] for a homogeneous population.

Global-to-local segmentation of the mid-cortical surface. The UKB served as the discovery cohort using a data-driven global-to-local segmentation of brain shape similar to previous work on face shape[7,111]. First, the superimposed and symmetrized mid-cortical surfaces were corrected using a partial least-squares regression (PLSR) with the function 'plsregress' in MATLAB 2019b for all UKB covariates listed above, augmented with centroid size to eliminate allometric effects of size on brain shape[91]. Second, pairwise structural connections based on the RV coefficient[112] between each pair of 3D surface vertices generated a squared similarity matrix (29,759 × 29,759). Third, a Laplacian transformation was applied to enhance similarities before eigendecomposition of this squared matrix. Finally, within the eigenvalue spectral map, we used *k*-means++ clustering to group highly correlated vertices that segment the brain into separate modules. This was performed in a bifurcating hierarchical manner using eight levels, resulting in a total of 511 hierarchically linked facial segments, with 1, 2, 4, 8, 16, 32, 64, 128 and 256 nonoverlapping modules at levels 0, 1, 2, 3, 4, 5, 6, 7 and 8. In contrast to our work on facial shape[7,111], we removed segments with fewer vertices than 1% of the total vertex count. This resulted in 285 segments across eight levels (Fig. 1). While the precise choice of number of hierarchical levels and vertex cutoff is arbitrary, the number of additional segments followed an 'elbow' trajectory, with few segments being retained at hierarchical levels greater than the ninth (Extended Data Fig. 2). Segmentation depth and cutoff criteria were determined before performing GWAS analysis. See Supplementary Note for details on the multivariate phenotyping approach within each brain segment.

Overlap of brain atlases with global-to-local segmentation. We investigated the overlap of brain segments at each of the eight levels from our global-to-local segmentation with brain regions from three commonly used brain atlases (Desikan-Killiany (34 distinct gyral-based regions)[32], Destrieux (74 distinct gyral- and sulcal-based regions)[33] and the Glasser (180 distinct multimodal-based regions)[34]). See Supplementary Note for details on computing overlap between our brain segments and brain atlases.

Global-to-local multivariate genome-wide discovery. The global-to-local phenotyping partitioned brain shape into overlapping (across different hierarchical levels) and nonoverlapping (within a single hierarchical level) segments, each of which was represented by a different subset of mid-cortical surface vertices and spanned by multiple dimensions of variation (PCs). See the Supplementary Note for details of the CCA-based approach used to discover SNP–phenotype associations.

A significance threshold of $P \leq 5 \times 10^{-8}$ was used to declare 'genome-wide significance', which corresponds to a Bonferroni correction for 1 million independent tests in a European-ancestry cohort[113]. Due to 285 multivariate GWAS runs, the multiple comparisons burden was magnified. Therefore, we also determined a more stringent threshold for declaring 'study-wide significance', which accounts for the effective number of independent tests. In a first instance, the number of eigenvalues larger than one of a pairwise multivariate correlation (RV coefficient) matrix (285 × 285)[114], determined a total of 210 independent tests. In a second instance, following the procedure by Kanai et al.[115], we obtained an empirical estimate of the number of independent tests using the 472 lead SNPs representing the genome-wide significant independent loci, to keep the estimations computationally tractable. See the Supplementary Note for details on empirical estimation of the number of independent tests.

Peak detection, overlap and annotations. We observed 38,630 SNPs and 23,413 SNPs at the level of genome-wide and study-wide significance, respectively. These were clumped into 472 (genome-wide) and 243 (study-wide) independent loci in three steps (Supplementary Note).

To study functional enrichment for genes near the 472 genome-wide lead SNPs, we performed Gene Ontology (GO) analysis using GREAT[43] (v4.0.4) and FUMA[42] (v1.3.6) with default settings. GO terms that were significant by both binomial and hypergeometric tests (FDR q value < 0.05) across three or two windows were reported as strongly and weakly enriched, respectively.

In determining overlap between lead SNPs from different GWASs, we used a similar strategy: two lead SNPs tag the same genetic locus if they are within 10 kb of each other or if they are within 1 Mb of each other and with an $r^2 > 0.2$. To quantify the overlap between the 472 brain shape loci and 430 other studies from the NHGRI-EBI GWAS Catalog, we defined LD blocks of 0.2 around the 472 loci using PLINK v1.9, and then calculated the OR and P value for the overlap between these blocks and any given GWAS using bedtools v2.27.1 with the fisher function.

In determining brain–face shared loci, we first considered the 472 genome-wide lead SNPs from the brain GWAS and looked for any SNP within 10 kb or within 1 Mb and LD > 0.2 of these lead SNPs with at least a genome-wide suggestive association ($P < 5 \times 10^{-7}$) association with face shape[111]. This resulted in 57 loci with evidence of association in brain and face shape. Then we took the 203 genome-wide lead SNPs reported in the face GWAS[111], and clumped them if two lead SNPs were within 10 kb or within 10 Mb with an $r^2 > 0.01$. For the resulting 197 independent genome-wide facial lead SNPs, we selected any SNP within 10 kb or within 1 Mb and with $r^2 > 0.2$ with at least suggestive ($P < 5 \times 10^{-7}$) association with brain shape. This resulted in another 54 loci with evidence of association in brain and face shape and, together with the previous 57 loci, they were clumped (within 10 kb or within 1 Mb and an $r^2 > 0.2$) into a final set of 76 brain–face shared loci.

We manually identified candidate genes in the vicinity of the 76 brain–face shared loci. For each locus, we first considered all genes within 500 kb of the lead SNP. We primarily relied on evidence for involvement of these genes in a human craniofacial or neurodevelopmental syndrome, or for evidence of craniofacial or neurodevelopmental defects in knockouts of their orthologs in mice. We also considered associations with GO terms related to craniofacial development, neurodevelopment or skeletal system development. In some cases (that is, *SOX9*, where enhancer–promoter interactions over 1 Mb have been described[52]), we extended the window to within 750 kb of the lead SNP.

Adolescent Brain Cognitive Development Study replication testing. The ABCD Study data were used for replication, with the UKB discovery cohort used as a phenotyping reference. First, after generalized Procrustes superimposition, the superimposed and symmetrized mid-cortical shapes were corrected for sex, age and the first five genetic PCs, augmented with centroid size to eliminate allometric effects of size on brain shape[91] using PLSR. Second, the PLSR residuals that were centered on average brain shape of the ABCD Study were added to the average brain shape of the UKB. Third, the corrected and re-centered brain shapes were segmented using global-to-local segmentation and projected onto the PCs of the UKB segments.

For each discovery lead SNP in a particular brain segment, the replication panel was projected onto the latent shape trait of the lead SNP. This generated univariate projection scores as phenotypes[116] to test for in the replication panel that are equivalent to the latent shape traits or phenotypes in the discovery panel. See the Supplementary Note for details on replication testing and FDR thresholds[117].

Clinical gene-panel overlap. Gene panels were downloaded from the Genomics England PanelApp website. Only panels used for clinical interpretation in the 100,000 Genomes Project were selected (provided by PanelApp[44]). The clinical gene panels were merged in disease (sub)categories according to the 100,000 Genomes Project criteria (for example, the clinical gene panel 'Intellectual Disability' belongs to the subcategory 'Neurodevelopmental Disorders', which is part of the 'Neurology and Neurodevelopment' disease category). Only genes with high confidence for gene–disease association were included in the clinical gene panels. See the Supplementary Note for details on calculation of gene set overlaps and significance.

Expression analyses of candidate genes at brain–face overlapping loci. Gene expression levels ($\log_2$(TPM) values) for 3D forebrain organoids and purified neuronal or glial lineages were obtained from Trevino et al.[53] (GSE132403). Raw RNA-sequencing reads from CNCCs at passages 1–4, as well as day 9 chondrocytes derived from P4 CNCCs, were obtained from Long et al.[52] (GSE145327), and TPM values were quantified using kallisto (v0.44.0)[118] with sequence-biased bias correction.

Linkage disequilibrium score regression SNP heritability for multivariate traits. In the Supplementary Note, we show that when applying LDSC to summary statistics of a multivariate GWAS, albeit with a small correction to the resulting χ^2 statistics, the heritability estimated by the LDSC slope is equal to $\frac{1}{D} trace\left(\Sigma_G \Sigma_P^{-1}\right)$, which is a D-dimensional generalization of heritability for genetic and phenotypic covariance matrices $\sum_G$ and $\sum_P$, respectively. When the dimensions of the multivariate trait are either genetically or phenotypically uncorrelated, this expression simplifies to the average SNP heritability across dimensions. Similarly, when applying S-LDSC, enrichments for partitioned average heritability are obtained. We further show that $\frac{1}{D} trace\left(\Sigma_G \Sigma_P^{-1}\right)$ is an appropriate multivariate generalization of heritability since it satisfies the following four properties: (1) invariance to units of measurement, (2) coordinate-free, (3) linear in $\sum_G$, and (4) maximized with a value of 1 when $\sum_G = \sum_P$.

Thus, for brain and face shape, we applied LDSC and S-LDSC using published software (https://github.com/bulik/ldsc/wiki/) to corrected χ^2 statistics from GWAS data of each brain or face segment. We used unmodified χ^2 values for the univariate traits analyzed (including indicated cases where we performed individual, univariate GWAS analysis for each brain and face shape PC). While using unmodified χ^2 values results in a small bias, we used unmodified statistics for consistency with previous studies. We limited S-LDSC analyses to traits with SNP-heritability z-scores > 7, as in the work of Finucaine et al.[67].

Functional annotations for stratified linkage disequilibrium score regression. We downloaded a range of publicly available cell-type and sample-specific annotations representing open chromatin and/or active regulatory regions. Specifically, we obtained data on open chromatin (all ATAC–seq peaks) from brain organoids[53], fetal brain tissue[119] and CNCCs and derived chondrocytes[52]. ATAC–seq reads from Long et al. were mapped to hg19 with bowtie2 (ref. [120]) with default settings, and peaks were called using MACS2 (ref. [121]) with default settings. Annotations for active regulatory regions (based on a range of epigenomic marks) were obtained from CNCCs[68], embryonic craniofacial tissues[69], fetal and adult brain tissue[70] and broad groupings of cell types[67]. For CNCCs[68], we combined all regions annotated as enhancers (weak, intermediate and strong) or promoters (weak and strong). For embryonic craniofacial tissues, we combined all regions with the following annotations from the 25-state chromHMM model: 'Enh', 'TxReg', 'PromD1', 'PromD2', 'PromU' and 'TssA'. For fetal and adult brain tissue, we combined all regions with the following annotations from the 15-state chromHMM model: '1_TssA', '2_TssAFlnk', '7_Enh' and '6_EnhG'. Each annotation was individually added to the baseline LD model from Finucaine et al. The resulting S-LDSC output (heritability fold-enrichment magnitude and significance and coefficient z-scores) is provided in Supplementary Data 2. When quantifying heritability enrichments with brain–face shared loci removed, we removed all SNPs within approximately the same independent LD block[122] as any of the 76 brain–face shared loci and recomputed LD scores.

Quantifying sharing of signals between pairs of GWAS. To assess the extent to which genome-wide profiles of association were shared between a pair of GWAS, we computed a Spearman correlation between two vectors of LD-block organized association P values. First, genome-wide SNPs were selected to overlap with the HapMap3 SNPs[123], and SNPs within the major histocompatibility complex region were removed. Second, we organized SNPs within 1,725 blocks in the human genome that can be treated as approximately independent in individuals of European ancestry[122]. For every LD block, we computed the mean SNP $-\log_{10}$(P value), and then computed a rank-based Spearman correlation using the averaged association value ($n = 1{,}725$) for each LD block. A standard error of the Spearman correlation was estimated using statistical resampling with 100 bootstrap cycles with replacement from the 1,725 LD blocks.

Ethics statement. This study was conducted in compliance with the principles of the Declaration of Helsinki, the principles of Good Clinical Practice and in accordance with all applicable regulatory requirements. Local ethics review and approval for this study (S63179) was performed and obtained from the ethical committee for research of the University Hospital UZ Leuven and the University KU Leuven.

Reporting Summary. Further information on research design is available in the Nature Research Reporting Summary linked to this article.

Data availability

All the data and detailed information for the UKB, including genetic markers, covariates and MRI images are available to bona fide researchers via the UKB data access process (http://www.ukbiobank.ac.uk/register-apply/).
All the data and detailed information for the ABCD Study, including genetic markers, covariates and MRI images are also available to bona fide researchers through the ABCD data depository (https://nda.nih.gov/abcd/request-access/; controlled access due to highly identifiable facial scans and brain MRIs linked to genotype data).
Relevant data and materials from the facial GWAS study are available online (https://doi.org/10.6084/m9.figshare.c.4667261)[124]. Full facial GWAS summary statistics are available from the NHGRI-EBI GWAS catalog (study accession GCST90007181). Furthermore, relevant files generated from the face and brain GWAS summary statistics as input to (S-)LDSC regression and Spearman correlations are available on FigShare (Supplementary Table 7). Full brain GWAS summary statistics are available from the GWAS catalog under prepublished/unpublished studies (accessions GCST90012880–GCST90013164, one accession number per brain segment). Gene expression data from 3D forebrain organoids (accession GSE132403) as well as CNCCs and derived chondrocytes (accession GSE145327) are available through the Gene Expression Omnibus.

All relevant additional data related to this work are provided in the FigShare repository for this work (https://doi.org/10.6084/m9.figshare.c.5089841.v1). This includes additional figures, input files and updated implementations, listed in Supplementary Table 7.

Code availability

MATLAB implementations of the hierarchical spectral clustering to obtain phenotypic shape segmentations are available from a previous publication (https://doi.org/10.6084/m9.figshare.7649024.v1)[7]. Updated implementations used in this work are provided in Supplementary Table 7. The statistical analyses in this work were based on functions of the statistical toolbox in MATLAB (Methods). Other materials and software used are available online. No other custom software packages were used.

References

85. Miller, K. L. et al. Multimodal population brain imaging in the UK Biobank prospective epidemiological study. *Nat. Neurosci.* **19**, 1523–1536 (2016).
86. Dale, A. M., Fischl, B. & Sereno, M. I. Cortical surface-based analysis. Segmentation and surface reconstruction. *Neuroimage* **9**, 179–194 (1999).
87. Dickie, E. W. et al. Ciftify: a framework for surface-based analysis of legacy MR acquisitions. *Neuroimage* **197**, 818–826 (2019).
88. Winkler, A. M. et al. Measuring and comparing brain cortical surface area and other areal quantities. *Neuroimage* **61**, 1428–1443 (2012).
89. Van Essen, D. C. A population-average, landmark- and surface-based (PALS) atlas of human cerebral cortex. *Neuroimage* **28**, 635–662 (2005).
90. Elliott, L. T. et al. Genome-wide association studies of brain imaging phenotypes in UK Biobank. *Nature* **562**, 210–216 (2018).
91. Zelditch, M. L., Swiderski, D. L. & Sheets, H. D. *Geometric Morphometrics for Biologists: a Primer* (Academic Press, 2012).
92. Eller, R. J., Janga, S. C. & Walsh, S. Odyssey: a semi-automated pipeline for phasing, imputation, and analysis of genome-wide genetic data. *BMC Bioinformatics* **20**, 364 (2019).
93. Delaneau, O., Zagury, J.-F., Robinson, M. R., Marchini, J. L. & Dermitzakis, E. T. Accurate, scalable and integrative haplotype estimation. *Nat. Commun.* **10**, 5436 (2019).
94. Rubinacci, S., Delaneau, O. & Marchini, J. Genotype imputation using the Positional Burrows Wheeler Transform. *PLoS Genet.* **16**, e1009049 (2020).
95. McCarthy, S. et al. A reference panel of 64,976 haplotypes for genotype imputation. *Nat. Genet.* **48**, 1279–1283 (2016).
96. Lam, M. et al. Comparative genetic architectures of schizophrenia in East Asian and European populations. *Nat. Genet.* **51**, 1670–1678 (2019).
97. Watson, H. J. et al. Genome-wide association study identifies eight risk loci and implicates metabo-psychiatric origins for anorexia nervosa. *Nat. Genet.* **51**, 1207–1214 (2019).
98. Stahl, E. A. et al. Genome-wide association study identifies 30 loci associated with bipolar disorder. *Nat. Genet.* **51**, 793–803 (2019).
99. Grove, J. et al. Identification of common genetic risk variants for autism spectrum disorder. *Nat. Genet.* **51**, 431–444 (2019).
100. Demontis, D. et al. Discovery of the first genome-wide significant risk loci for attention deficit/hyperactivity disorder. *Nat. Genet.* **51**, 63–75 (2019).
101. Jansen, I. E. et al. Genome-wide meta-analysis identifies new loci and functional pathways influencing Alzheimer's disease risk. *Nat. Genet.* **51**, 404–413 (2019).
102. Jansen, P. R. et al. Genome-wide analysis of insomnia in 1,331,010 individuals identifies new risk loci and functional pathways. *Nat. Genet.* **51**, 394–403 (2019).
103. Nagel, M. et al. Meta-analysis of genome-wide association studies for neuroticism in 449,484 individuals identifies novel genetic loci and pathways. *Nat. Genet.* **50**, 920–927 (2018).
104. Savage, J. E. et al. Genome-wide association meta-analysis in 269,867 individuals identifies new genetic and functional links to intelligence. *Nat. Genet.* **50**, 912–919 (2018).
105. Bradfield, J. P. et al. A genome-wide meta-analysis of six type 1 diabetes cohorts identifies multiple associated loci. *PLoS Genet.* **7**, e1002293 (2011).
106. Stahl, E. A. et al. Genome-wide association study meta-analysis identifies seven new rheumatoid arthritis risk loci. *Nat. Genet.* **42**, 508–514 (2010).
107. López-Isac, E. et al. GWAS for systemic sclerosis identifies multiple risk loci and highlights fibrotic and vasculopathy pathways. *Nat. Commun.* **10**, 4955 (2019).
108. Jin, Y. et al. Genome-wide association studies of autoimmune vitiligo identify 23 new risk loci and highlight key pathways and regulatory variants. *Nat. Genet.* **48**, 1418–1424 (2016).
109. Li, J. et al. Robust genome-wide ancestry inference for heterogeneous datasets and ancestry facial imaging based on the 1000 Genomes Project. Preprint at *bioRxiv* https://doi.org/10.1101/549881 (2019).
110. Yang, J., Lee, S. H., Goddard, M. E. & Visscher, P. M. GCTA: a tool for genome-wide complex trait analysis. *Am. J. Hum. Genet.* **88**, 76–82 (2011).
111. White, J. D. et al. Insights into the genetic architecture of the human face. *Nat. Genet.* **53**, 45–53 (2021).
112. Robert, P. & Escoufier, Y. A unifying tool for linear multivariate statistical methods: the RV coefficient. *J. R. Stat. Soc. Ser. C Appl. Stat.* **25**, 257–265 (1976).
113. Pe'er, I., Yelensky, R., Altshuler, D. & Daly, M. J. Estimation of the multiple testing burden for genome-wide association studies of nearly all common variants. *Genet. Epidemiol.* **32**, 381–385 (2008).
114. Li, J. & Ji, L. Adjusting multiple testing in multilocus analyses using the eigenvalues of a correlation matrix. *Heredity (Edinb.)* **95**, 221–227 (2005).
115. Kanai, M., Tanaka, T. & Okada, Y. Empirical estimation of genome-wide significance thresholds based on the 1000 Genomes Project dataset. *J. Hum. Genet.* **61**, 861–866 (2016).
116. Claes, P. et al. Modeling 3D facial shape from DNA. *PLoS Genet.* **10**, e1004224 (2014).
117. Benjamini, Y. & Yekutieli, D. The control of the false discovery rate in multiple testing under dependency. *Ann. Stat.* **29**, 1165–1188 (2001).
118. Bray, N. L., Pimentel, H., Melsted, P. & Pachter, L. Near-optimal probabilistic RNA-seq quantification. *Nat. Biotechnol.* **34**, 525–527 (2016).
119. de la Torre-Ubieta, L. et al. The dynamic landscape of open chromatin during human cortical neurogenesis. *Cell* **172**, 289–304 (2018).
120. Langmead, B., Trapnell, C., Pop, M. & Salzberg, S. L. Ultrafast and memory-efficient alignment of short DNA sequences to the human genome. *Genome Biol.* **10**, R25 (2009).
121. Zhang, Y. et al. Model-based analysis of ChIP–Seq (MACS). *Genome Biol.* **9**, R137 (2008).
122. Berisa, T. & Pickrell, J. K. Approximately independent linkage disequilibrium blocks in human populations. *Bioinformatics* **32**, 283–285 (2016).
123. Altshuler, D. M. et al. Integrating common and rare genetic variation in diverse human populations. *Nature* **467**, 52–58 (2010).
124. Naqvi, S. Shared heritability of face and brain shape. *figshare* https://doi.org/10.6084/m9.figshare.c.5089841.v1 (2021).

Acknowledgements

J.W. was supported by the Howard Hughes Medical Institute, a Lorry Lokey endowed professorship and a Stinehart Reed award. S.N. was supported by a Helen Hay Whitney Fellowship. The KU Leuven research team and analyses were supported by the National Institutes of Health (NIH; 1-R01-DE027023 and 2-R01-DE027023), The Research Fund KU Leuven (BOF-C1, C14/15/081 and C14/20/081) and The Research Program of the Research Foundation in Flanders (FWO; G078518N). The computational resources and services used in this work were provided by the VSC (Flemish Supercomputer Center), funded by the FWO and the Flemish Government (department EWI). J.P.S. was supported by an NIH training grant (5T32HG000044-23). J.K.P. was supported by the NIH (HG008140 and HG009431). Pittsburgh personnel, data collection and analyses were supported by the National Institute of Dental and Craniofacial Research (U01-DE020078, R01-DE016148 and R01-DE027023). Funding for genotyping by the National Human Genome Research Institute (X01-HG007821 and X01-HG007485) and funding for initial genomic data cleaning by the University of Washington were provided by contract HHSN268201200008I from the National Institute for Dental and Craniofacial Research awarded to the Center for Inherited Disease Research (https://www.cidr.jhmi.edu/). J.T. was supported by the NIH (5R01-DA033431-07) and the National Science Foundation (1922598). This research has been conducted, in part, using the UKB resource under application no. 43193 (understanding the genetic architecture of human brain shape from MRI using global-to-local shape segmentations), and we are grateful for all the participants in that resource. This manuscript reflects the views of the authors and may not reflect the opinions or views of the UKB funders and investigators. Data used in the preparation of this article were obtained from the ABCD Study (https://abcdstudy.org), held in the National Institute of Mental Health Data Archive. This is a multisite, longitudinal study designed to recruit more than 10,000 children aged 9–10 years and follow them over 10 years into early adulthood. The ABCD Study is supported by the NIH and additional federal partners under award nos. U01DA041022, U01DA041028, U01DA041048, U01DA041089, U01DA041106, U01DA041117, U01DA041120, U01DA041134, U01DA041148, U01DA041156, U01DA041174, U24DA041123, U24DA041147, U01DA041093 and U01DA041025. A full list of supporters is available at https://abcdstudy.org/federal-partners.html. A list of participating sites and study investigators can be found at https://abcdstudy.org/wp-content/uploads/2019/04/Consortium_Members.pdf. ABCD consortium investigators provided data but did not necessarily participate in analysis or writing of this report. This manuscript reflects the views of the authors and may not reflect the opinions or views of the NIH or ABCD consortium investigators.

Author contributions

Conceptualization: P.C., J.W. and S.N.; methodology: J.P.S., P.C. and J.T.; software: P.C., H.H., K.I., R.J.E., J.T., S.N. and Y.S.; formal analysis: J.P.S. and P.C.; investigation: S.N.,

Y.S., P.C., R.B. and A.R.; resources: S.R., M.D.S., J.R.S., S.M.W., S.W. and P.C.; data curation: S.N., Y.S., P.C., H.H. and K.I.; writing—original draft: S.N., Y.S., H.P., J.W., P.C., A.R., S.S. and R.B.; writing—review and editing: H.P., Y.S., H.H., K.I., J.T., J.K.P., J.P.S., S.W., S.M.W., J.R.S., M.D.S. and R.J.E.; visualization: P.C., Y.S., S.N. and A.R.; supervision: P.C., J.W., H.P., S.S., J.K.P. and S.W.; project administration: P.C., J.W., H.P., S.W., S.R., M.D.S., J.R.S. and S.M.W.; funding acquisition: P.C., J.W., H.P., S.W., S.R., M.D.S., J.R.S. and S.M.W.

Competing interests

The authors declare no competing interests.

Additional information

Extended data is available for this paper at https://doi.org/10.1038/s41588-021-00827-w.

Supplementary information The online version contains supplementary material available at https://doi.org/10.1038/s41588-021-00827-w.

Correspondence and requests for materials should be addressed to S.N., J.W. or P.C.

Peer review information *Nature Genetics* thanks Christopher Walsh and the other, anonymous, reviewer(s) for their contribution to the peer review of this work. Peer reviewer reports are available.

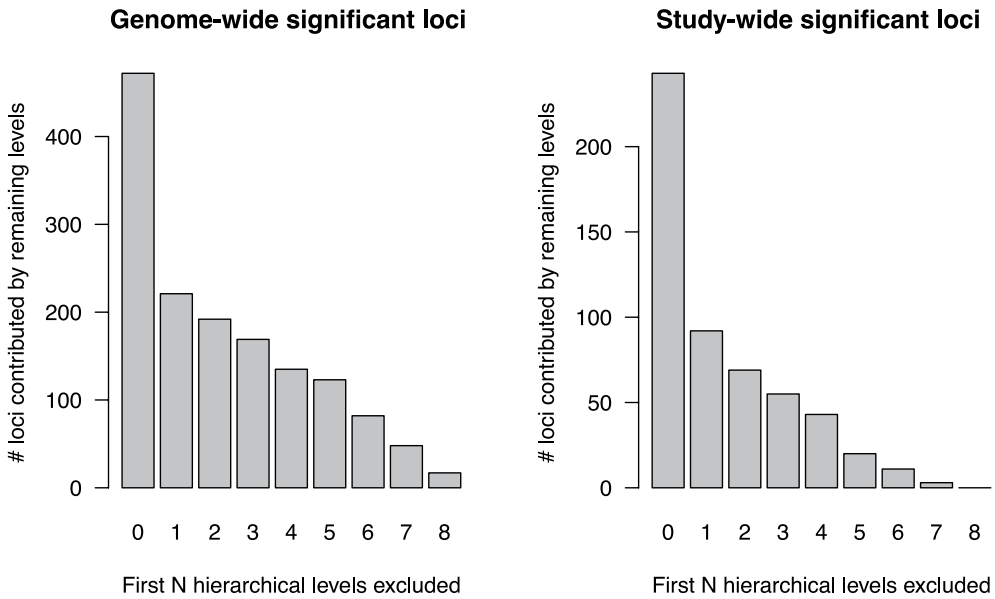

Extended Data Fig. 1 | Number of additional brain shape loci contributed by hierarchical levels. For all genome-wide (left) or study-wide (right) significant associations, associations with all segments in hierarchical levels up to the indicated number were masked, and the number of remaining associations was assessed.

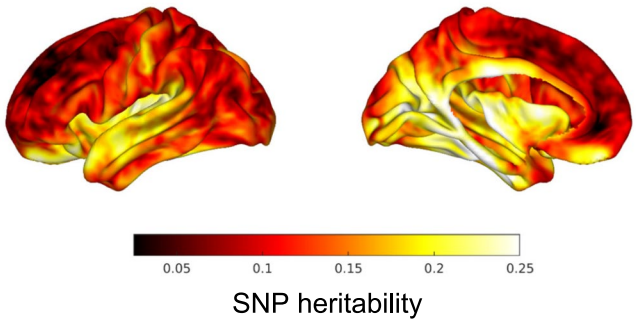

Extended Data Fig. 2 | Point-wise SNP heritability estimates across the mid-cortical surface. Colors represent the total SNP heritability (computed by a linear mixed model approach, see Methods) at each point on the mid-cortical surface, represented by a set of three-dimensional coordinates in each individual.

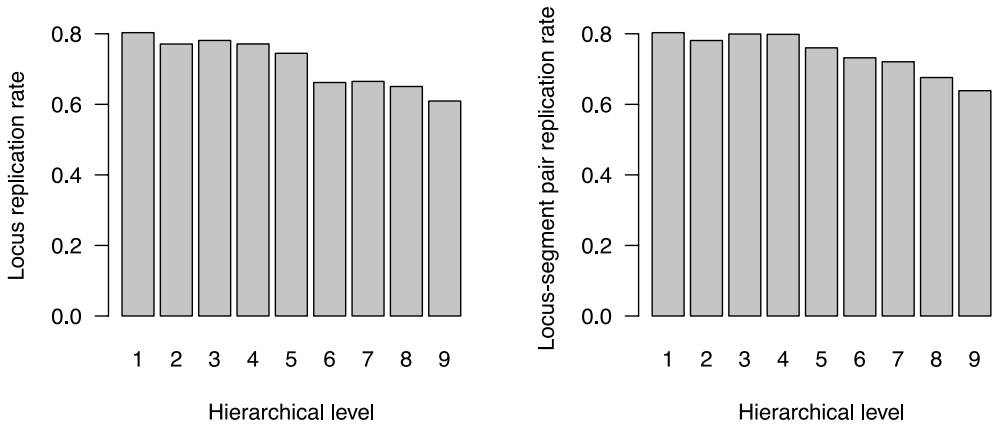

Extended Data Fig. 3 | Replication rates in the ABCD cohort by hierarchical level. Only segments in the indicated hierarchical level were considered, and all loci (left) or locus-segment pairs (right) reaching genome-wide significance in those segments were tested for replication in the ABCD cohort at a 5% FDR.

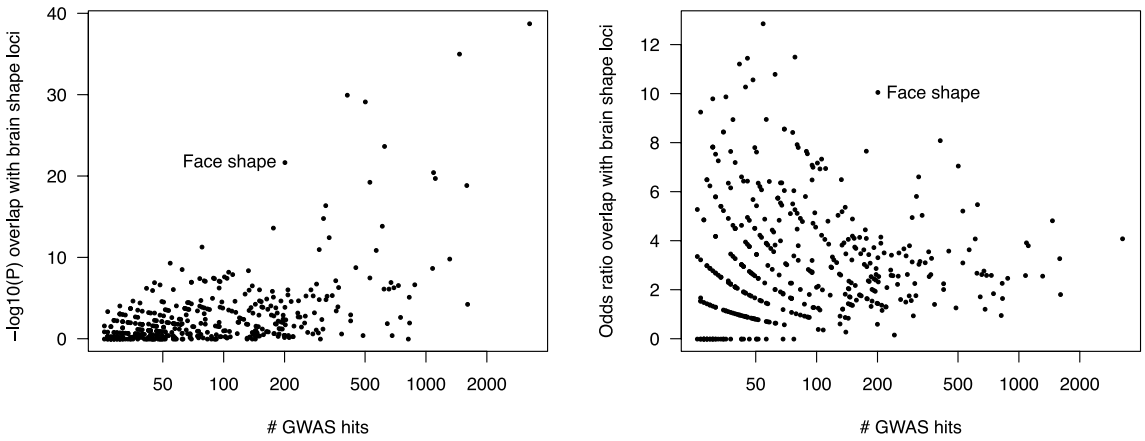

Extended Data Fig. 4 | Overlap between genome-wide significant brain shape loci and genome-wide significant loci from 430 other studies. GWAS hits (number on x-axis) for other studies were obtained from the NCBI-EBI GWAS Catalog, and *P*-values (left, y-axis) and odds ratios (right, y-axis) for significance of overlap with regions in LD (> 0.2) with brain shape loci were computed using bedtools' fisher function (see Methods). Note that relative to other traits with equivalent numbers of GWAS hits, face shape shows overlap with brain shape loci greater in both significance and magnitude.

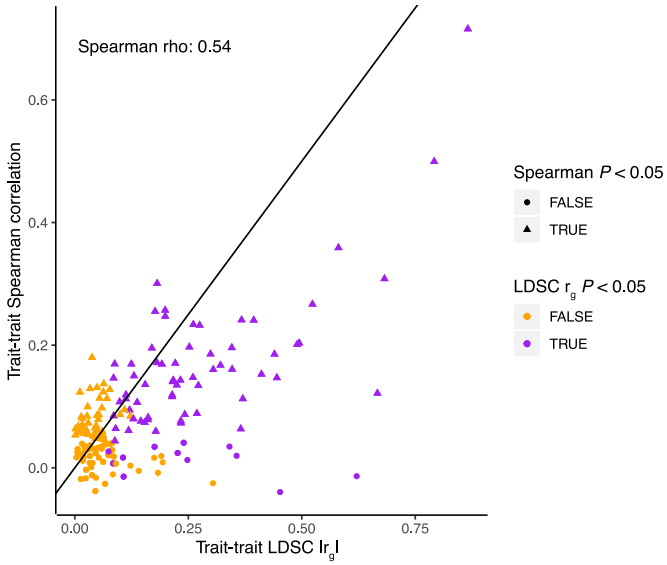

Extended Data Fig. 5 | Comparison of LDSC genetic correlations and Spearman correlation between pairs of univariate traits. Each point represents a pair of univariate traits (of all those considered in this study, see Methods), while the x- and y-axes indicate the absolute value of the LDSC-estimated genetic correlation and the estimated genome-wide sharing of effects by the Spearman correlation method. Point colors and shapes indicate significance ($P < 0.05$) from LDSC or the Spearman correlation method, respectively. Exact p-values are provided in Supplementary Table 6.

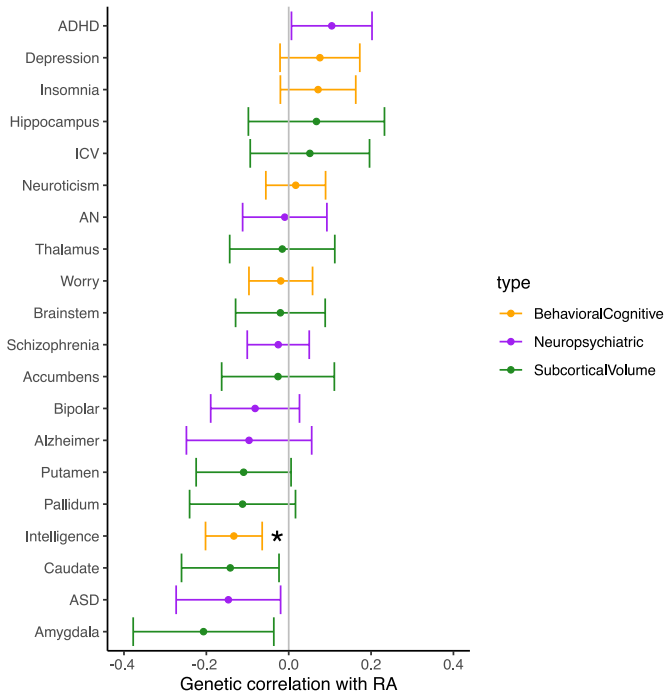

Extended Data Fig. 6 | Genetic correlations between RA (rheumatoid arthritis) and univariate brain-related traits. Points (center of error bars) represent estimated genetic correlations. Error bars represent 95% confidence intervals. *, 5% FDR.

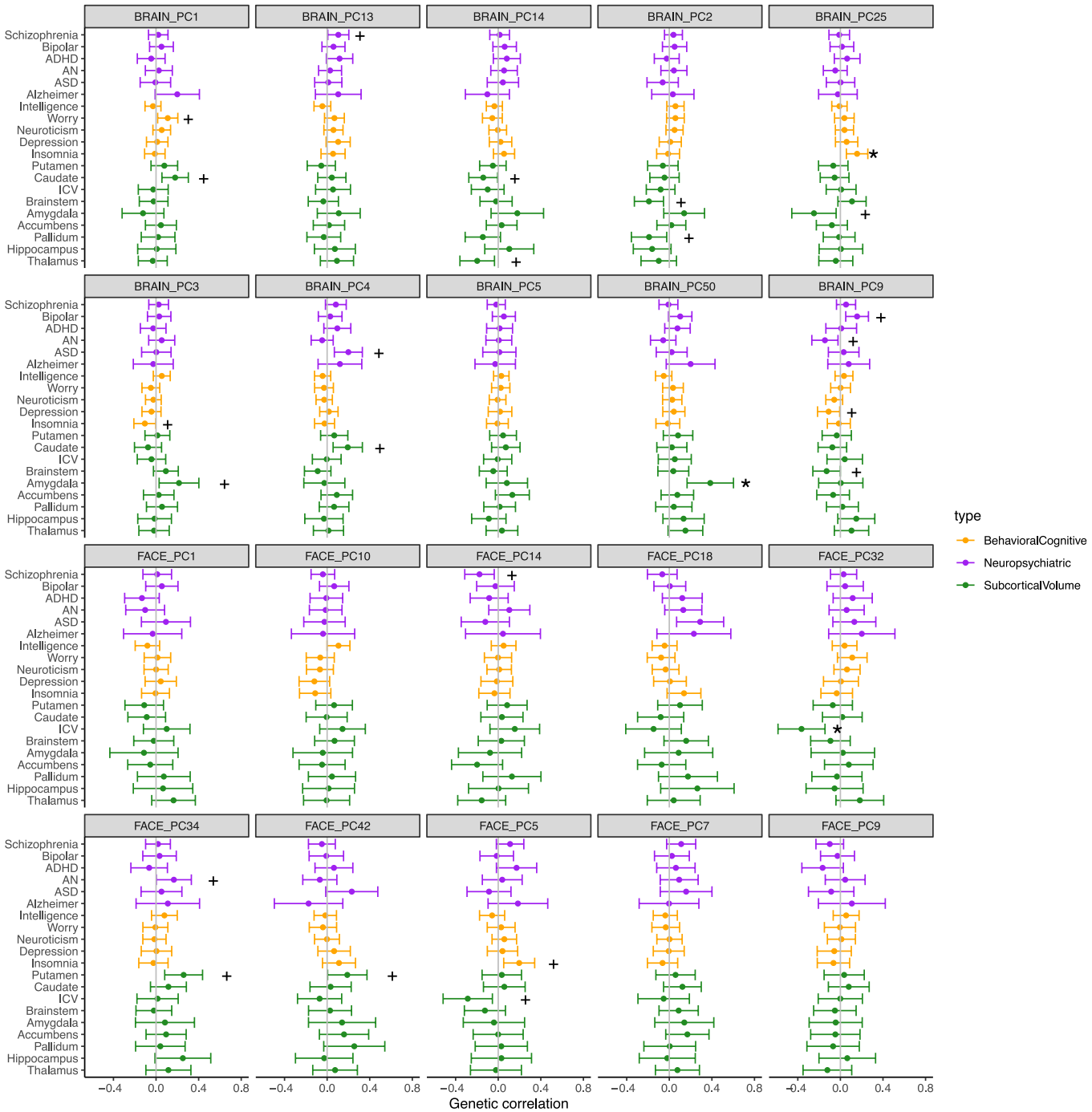

Extended Data Fig. 7 | Genetic correlations between the most heritable brain (top two rows) or face (bottom two rows) shape PCs and other traits. Points (center of error bars) represent estimated genetic correlations (r_g) between the top ten shape PCs (for segment 1, the full brain or face) with heritability z-score > 3 and each of the indicated univariate traits using LD score regression. Error bars represent 95% confidence intervals. *, 5% FDR for indicated PC; +, 10% FDR.

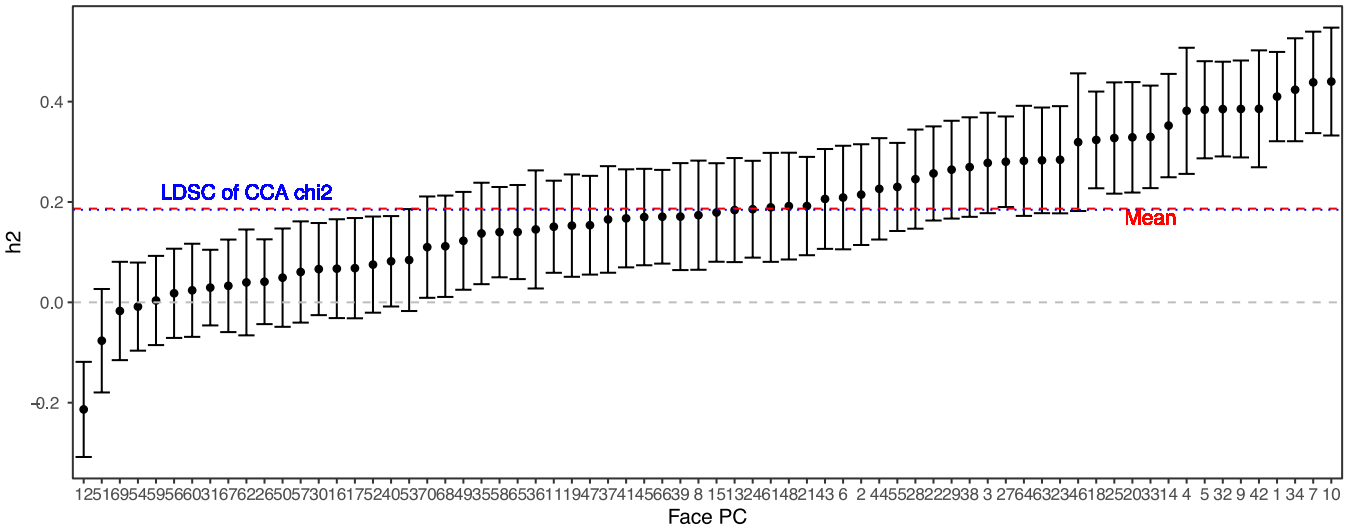

Extended Data Fig. 8 | SNP heritability of individual face shape PCs and multivariate face shape estimated by LDSC. Points (center of error bars) represent estimated SNP heritability of each PC. Error bars represent 95% confidence intervals. The red line represents the mean heritability of all 70 PCs, and the blue line indicates the heritability obtained by applying LDSC to corrected χ^2 statistics from the multivariate CCA GWAS using all 70 PCs.

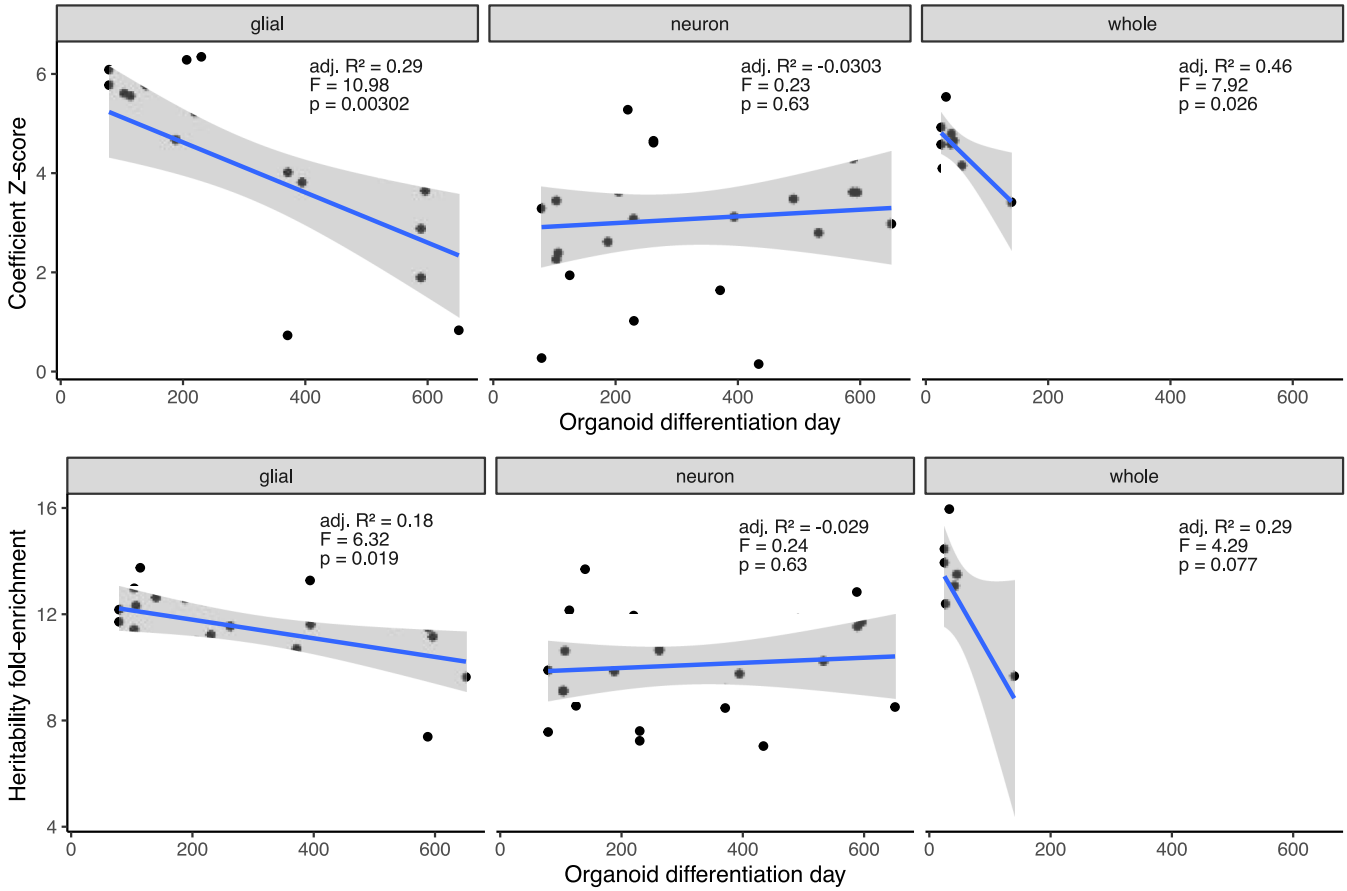

Extended Data Fig. 9 | Partitioned heritability enrichments for brain shape with respect to stage- and cell-type-specific brain organoid open chromatin. S-LDSC coefficient Z-scores and heritability fold-enrichment for annotations corresponding to the indicated cell-type and differentiation day were computed as described in Methods. Regression lines represent the linear best fit with intercept and organoid differentiation day as dependent variable, and grey areas represent 95% confidence intervals. P-values are from a two-tailed F-test.

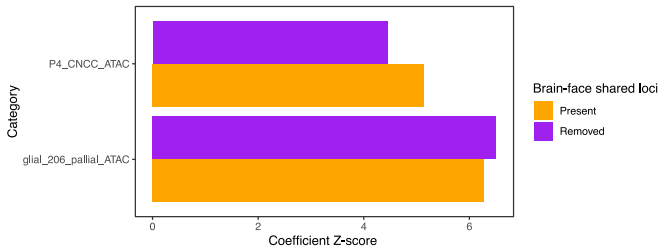

Extended Data Fig. 10 | Partitioned heritability enrichments for brain shape with respect to open chromatin in CNCCs or early glial organoid cells, with or without 76 brain-face shared loci. S-LDSC Z-scores were calculated using full brain shape as the trait and the most enriched craniofacial (top) or brain organoid (bottom) ATAC-seq dataset as annotations. Z-scores were re-estimated (blue) after removing all SNPs in the same approximately independent LD block as one of the 76 brain-face shared loci (see Methods for details).

nature research

Corresponding author(s): Peter Claes, Joanna Wysocka, Sahin Naqvi

Last updated by author(s): Jan 15, 2021

Reporting Summary

Nature Research wishes to improve the reproducibility of the work that we publish. This form provides structure for consistency and transparency in reporting. For further information on Nature Research policies, see our Editorial Policies and the Editorial Policy Checklist.

Statistics

For all statistical analyses, confirm that the following items are present in the figure legend, table legend, main text, or Methods section.

n/a	Confirmed	
☐	☒	The exact sample size (*n*) for each experimental group/condition, given as a discrete number and unit of measurement
☐	☒	A statement on whether measurements were taken from distinct samples or whether the same sample was measured repeatedly
☐	☒	The statistical test(s) used AND whether they are one- or two-sided *Only common tests should be described solely by name; describe more complex techniques in the Methods section.*
☐	☒	A description of all covariates tested
☐	☒	A description of any assumptions or corrections, such as tests of normality and adjustment for multiple comparisons
☐	☒	A full description of the statistical parameters including central tendency (e.g. means) or other basic estimates (e.g. regression coefficient) AND variation (e.g. standard deviation) or associated estimates of uncertainty (e.g. confidence intervals)
☐	☒	For null hypothesis testing, the test statistic (e.g. *F*, *t*, *r*) with confidence intervals, effect sizes, degrees of freedom and *P* value noted *Give P values as exact values whenever suitable.*
☒	☐	For Bayesian analysis, information on the choice of priors and Markov chain Monte Carlo settings
☐	☒	For hierarchical and complex designs, identification of the appropriate level for tests and full reporting of outcomes
☐	☒	Estimates of effect sizes (e.g. Cohen's *d*, Pearson's *r*), indicating how they were calculated

Our web collection on statistics for biologists contains articles on many of the points above.

Software and code

Policy information about availability of computer code

Data collection	No software was used for data collection as part of this study.
Data analysis	Matlab implementations of the hierarchical spectral clustering to obtain phenotypic shape segmentations are available from a previous publication https://doi.org/10.6084/m9.figshare.7649024.v1). Updated implementations used in this work are provided, (https://doi.org/10.6084/m9.figshare.c.5089841.v1). The statistical analyses in this work were based on functions of the statistical toolbox in Matlab as mentioned throughout the Methods. Other materials and external software used mentioned throughout the methods, are all available online (see URL section). The following versions of software were used: SHAPEIT4, IMPUTE5, plink 1.9, bowtie2, MACS2, bedtools v2.27.1, kallisto v0.44.0, FreeSurfer v6.0.0

For manuscripts utilizing custom algorithms or software that are central to the research but not yet described in published literature, software must be made available to editors and reviewers. We strongly encourage code deposition in a community repository (e.g. GitHub). See the Nature Research guidelines for submitting code & software for further information.

Data

Policy information about availability of data

All manuscripts must include a data availability statement. This statement should provide the following information, where applicable:

- Accession codes, unique identifiers, or web links for publicly available datasets
- A list of figures that have associated raw data
- A description of any restrictions on data availability

All the data and detailed information for the UK Biobank, including genetic markers, covariates and MRI images are available to bona fide researchers via the UK Biobank data access process (see http://www.ukbiobank.ac.uk/register-apply/).
All the data and detailed information for the ABCD study, including genetic markers, covariates and MRI images are also available to bona fide researchers through

the ABCD data depository (https://nda.nih.gov/abcd/request-access)
Relevant data and materials from the facial GWAS study are available online (https://doi.org/10.6084/m9.figshare.c.4667261). The full facial GWAS summary statistics are available on the NHGRI-EBI GWAS catalog (study accession GCST90007181). Furthermore, relevant files generated from the face and brain GWAS summary statistics as input to (S-)LDSC regression and spearman correlations are available on FigShare, see Supplementary Table 8. The full brain GWAS summary statistics are available on the GWAS catalog (study accession GCST90012882).

All relevant additional data related to this work are provided in the FigShare repository for this work (https://doi.org/10.6084/m9.figshare.c.5089841.v1). This includes additional figures, input files and updated implementations, listed in Supplementary Table 8.

Field-specific reporting

Please select the one below that is the best fit for your research. If you are not sure, read the appropriate sections before making your selection.

☒ Life sciences ☐ Behavioural & social sciences ☐ Ecological, evolutionary & environmental sciences

For a reference copy of the document with all sections, see nature.com/documents/nr-reporting-summary-flat.pdf

Life sciences study design

All studies must disclose on these points even when the disclosure is negative.

Sample size	No statistical method was used to predetermine sample size. Sample sizes were determined to be sufficient based on results of previous GWAS of brain phenotypes with similar sample sizes. Sample size was maximized based on data availability in the UK Biobank, after excluding samples that failed image processing, were outliers with respect to covariates, or had non-European ancestry.
Data exclusions	MRI images were excluded if they failed any steps of the surface reconstruction and segmentation pipeline, as described in detail in Methods. Individuals with extreme outlier values for certain covariates were excluded, as described in Methods. Individuals of primarily non-European descent as well as related individuals were excluded, as described in Methods. These exclusionary measures were determined prior to performing GWAS analysis.
Replication	Effects of the 472 genome-wide significant loci for brain shape were subject to a single replication analysis using MRI images from the ABCD cohort. Of the 472 loci, 466 were available for testing in the ABCD cohort after imputation and filtering. Of these 466, 305 (65.4%) replicated at least one associated segment at 5% FDR.
Randomization	MRI images were assigned into groups based on SNP genotypes. Images were adjusted for sex, age, height, weight, diastolic and systolic blood pressures, and 10 principal components representing ancestry components.
Blinding	Investigators were not blinded to group allocation. While individual genotypes had to be accessed to perform quality control and filtering, the group allocation was based on individual genotypes and so could not be changed.

Reporting for specific materials, systems and methods

We require information from authors about some types of materials, experimental systems and methods used in many studies. Here, indicate whether each material, system or method listed is relevant to your study. If you are not sure if a list item applies to your research, read the appropriate section before selecting a response.

Materials & experimental systems

n/a	Involved in the study	
☒	☐	Antibodies
☒	☐	Eukaryotic cell lines
☒	☐	Palaeontology and archaeology
☒	☐	Animals and other organisms
☐	☒	Human research participants
☒	☐	Clinical data
☒	☐	Dual use research of concern

Methods

n/a	Involved in the study	
☒	☐	ChIP-seq
☒	☐	Flow cytometry
☐	☒	MRI-based neuroimaging

Human research participants

Policy information about studies involving human research participants

Population characteristics	The UK Biobank project (UKB) is a large dataset of about 500,000 British volunteers with informed consent containing genetics, non-imaging variables and brain imaging data acquired using a fixed protocol
Recruitment	Participants were recruited by the UK Biobank. Selection bias in the UK Biobank has been observed to favor healthy, European-ancestry individuals.

Ethics oversight	This study was conducted in compliance with the principles of the Declaration of Helsinki, the principles of GCP and in accordance with all applicable regulatory requirements. Local ethics review and approval for this study (S63179) was performed and obtained from the ethical committee for research of the University Hospital UZ Leuven and the University KU Leuven. Collection of the data in the UK Biobank was governed by the Ethics and Governance Council of the UK Biobank.

Note that full information on the approval of the study protocol must also be provided in the manuscript.

Magnetic resonance imaging

Experimental design

Design type	Resting state
Design specifications	https://biobank.ctsu.ox.ac.uk/crystal/crystal/docs/brain_mri.pdf
Behavioral performance measures	Not applicable

Acquisition

Imaging type(s)	T1-weighted structural imaging
Field strength	3T
Sequence & imaging parameters	page 8 in https://biobank.ctsu.ox.ac.uk/crystal/crystal/docs/brain_mri.pdf
Area of acquisition	Whole brain scan

Diffusion MRI ☐ Used ☒ Not used

Preprocessing

Preprocessing software	Standard T1 preprocessing steps are described on page 12-13 in https://biobank.ctsu.ox.ac.uk/crystal/crystal/docs/brain_mri.pdf. Followed by Freesurfer recon-all and ciftify as described in the methods
Normalization	page 12-13 in https://biobank.ctsu.ox.ac.uk/crystal/crystal/docs/brain_mri.pdf
Normalization template	T1 preprocessing involved the MNI152 template (page 12-13 in https://biobank.ctsu.ox.ac.uk/crystal/crystal/docs/brain_mri.pdf). Ciftify output used is based on the low resolution Conte69 cortical surface template for left and right hemisphere as described in the methods.
Noise and artifact removal	Freesurfer embedded noise and artifact removal. Additional imaging covariates, volumetric scaling from T1 head image to standard space, XYZ-position of brain mask in scanner co-ordinates, Z-position of table/coil in scanner co-ordinates, date of attending assessment center, and assessment center were used to correct the brain surface data using partial least square regression.
Volume censoring	Not applicable

Statistical modeling & inference

Model type and settings	Multivariate shape analysis
Effect(s) tested	Fixed effects of SNP genotypes on multivariate shape variables

Specify type of analysis: ☐ Whole brain ☐ ROI-based ☒ Both

Anatomical location(s)	Hierarchical data-driven shape segmentation as described in the methods and applied elsewhere on 3D facial shapes
Statistic type for inference (See Eklund et al. 2016)	Surface-based and not voxel-based multivariate shape variables, subjected to association with SNP genotypes using canonical correlation analysis
Correction	Correction of multivariate shape variables for covariates was performed using partial least squares regression. Correction for multiple testing was performed based on permutations, followed by an adjusted study-wide p-value threshold by devision of the less stringent genome-wide threshold by the effective number of tests.

Models & analysis

n/a	Involved in the study
☒	☐ Functional and/or effective connectivity
☒	☐ Graph analysis
☐	☒ Multivariate modeling or predictive analysis

Multivariate modeling and predictive analysis

For each of the 285 brain segments separately, the group of 3D surface vertices in a segment were subjected to a new GPA. As such, a multivariate shape-space for each brain segment was constructed independently of the other segments and its relative positioning within the full brain hemisphere. Subsequently, after GPA, each segment's shape-space was spanned by a multivariate orthogonal basis using PCA on the pooled x, y and z coordinates of the collection of superimposed vertices in that segment. Finally, we retained enough PCs to explain up to 80% of the total shape variation within each segment. Associations of multivariate shape spaces with SNP genotypes were tested using canonical correlation analysis.